

Electronic Thesis and Dissertation Repository

---

4-21-2020 4:00 PM

## The of Application of 3D-Printing to Lumbar Spine Surgery

Andrew J. Kanawati, *The University of Western Ontario*

Supervisor: Dr Parham Rasoulinejad, *The University of Western Ontario*

A thesis submitted in partial fulfillment of the requirements for the Master of Science degree in Surgery

© Andrew J. Kanawati 2020

Follow this and additional works at: <https://ir.lib.uwo.ca/etd>



Part of the [Biomedical Devices and Instrumentation Commons](#), [Musculoskeletal System Commons](#), [Orthopedics Commons](#), and the [Surgery Commons](#)

---

### Recommended Citation

Kanawati, Andrew J., "The of Application of 3D-Printing to Lumbar Spine Surgery" (2020). *Electronic Thesis and Dissertation Repository*. 7030.  
<https://ir.lib.uwo.ca/etd/7030>

This Dissertation/Thesis is brought to you for free and open access by Scholarship@Western. It has been accepted for inclusion in Electronic Thesis and Dissertation Repository by an authorized administrator of Scholarship@Western. For more information, please contact [wlsadmin@uwo.ca](mailto:wlsadmin@uwo.ca).

# **The of Application of 3D-Printing to Lumbar Spine Surgery**

Andrew Kanawati

BSc MBBS (Hons) 2006, Mast Anat UNE 2015, FRACS Orth 2018

## Abstract

3D-printing refers to the manufacturing process in which a three-dimensional (3D) digital model can be transformed into a physical model by layering material in the shape of successive cross sections atop of previously layers. 3D-printing has been increasing in popularity in the field of medicine and surgery due to the ability to personalize various aspects of patient care. This thesis will explore the application of 3D-printing to lumbar spine surgery, aiming to quantify the accuracy of medical imaging when relating to imaged structures and their corresponding models produced by 3D-printing, and determine if complex patient-specific guides are accurate and safe.

## Summary for Lay Audience

Three-dimensional printing (3D-printing) is a new tool that is being used in spine surgery. Patients with spinal conditions undergo medical imaging investigations, especially if they require surgery. Two types of imaging techniques routinely used are: 1) Computed tomography (CT) and 2) magnetic resonance imaging (MRI). Each technique has its own advantages and disadvantages. CT provides excellent bone detail; however, soft tissue (muscle, nerve, spinal cord) detail is limited and CT scans require moderate doses of radiation to acquire. Magnetic resonance imaging (MRI), on the other hand, provides excellent soft tissue details and requires no radiation to acquire, but the detail of bony structures is limited. 3D-printed models of the spine, with guides to direct screws in place, are increasingly being created to help with planning surgeries. Previous studies have used CT to acquire 3D data for 3D-printing of the spinal structures. However, this has never been done using MRI because it has been too difficult to assess the bones. It would be advantageous to use MRI data because the majority of patients have an MRI before spine surgery, and patients would be exposed to less radiation when compared to CT. MRI cannot be performed on some patients with anxiety, and is not possible when some metallic implants are present.

The rationale for this study is to investigate if an evolving MRI technique ('Blackbone' MRI) can acquire enough bone detail to then be used to 3D print guides to assist surgeons during operations. This would mean that CT scans for spine surgery, and the radiation that comes with them, may no longer be needed.

There are no studies so far looking at whether MRI can provide information to build patient-specific guides to assist spine surgeons. This would mean that MRI scans could be performed to

benefit the patient and give information about their condition, as well as plan for their surgery with 3D printed guides.

The research question is: can 3D-printed patient specific guides be produced from MRI?

This research will determine if accurate guides can be produced using MRI scans. These guides help surgeons to increase accuracy and speed of their surgery. If accurate guides can be produced using MRI scans, then CT scans, performed either before or during surgery, will be needed less frequently. This will reduce the radiation exposure for patients and surgical teams.

This experimental study will involve performing MRI scans of bones of the spine from people that have donated their bodies for research. These MRI scans will then be used to build surgical guides which will be tested for accuracy. Patient-specific guides are a relatively cheap, and effective way of improving surgical outcomes.

This research will be informative to Orthopedic and Neurosurgical spine surgeons with the first evidence to date regarding this subject. The results of this study will draw the attention of the scientific community to an important topic regarding surgical complications, that occurs in approximately 10% of spine surgeries. It will pave the way for future research to make the applicability of this technique possible, bringing better surgical results for patients, improve patient's expectations and a lower cost in terms of health of populations.

**AUTHOR'S DECLARATION FOR ELECTRONIC SUBMISSION OF A THESIS**

I hereby declare that I am the sole author of this thesis. This is a true copy of the thesis.

I authorize Western University to lend this thesis to other institutions or individuals for the purposes of scholarly research.

I further authorize Western University to reproduce this thesis by photocopying or by other means, in total or in part, at the request of other institutions or individuals for the purpose of scholarly research.

I understand that my thesis may be made electronically available to the public.

## Acknowledgements

I would like to thank several people for special contributions to this project.

To my supervisors, Dr Parham Rasoulinejad and Dr Chris Bailey, for their expert opinions at every stage of the evolution of this project.

To Aaron Gee and Dr Renan Fernandes for their assistance with 3D scanning, additive manufacturing and testing of the guides.

To Dr Jennifer Urquhart for her assistance and expertise in the statistical analysis.

To Dave Reese, from Robarts Research Institute, for his assistance and expertise in obtaining the MRI scans.

To Haley Linklater and the staff from the Body Bequeathal Program.

To Dr Andas Lasso and members of the 3D Slicer development team.

I would also like to thank my thesis review committee, Dr Hassan Razvi, Dr George Athwal, Dr Brent Lanting, and Dr Wankei Wan. Thank you for taking the time to review my thesis.

## Dedication

To my loving and devoted wife Juliana, my daughter Elena, and to my parents Maria and Nayef Kanawati.

## Table of Contents

ABSTRACT.....	I
SUMMARY FOR LAY AUDIENCE.....	II
ACKNOWLEDGEMENTS.....	V
DEDICATION.....	VI
TABLE OF CONTENTS.....	VII
DECLARATION OF CONFLICTING INTERESTS.....	IX
FUNDING.....	IX
CONTRIBUTIONS.....	IX
ABBREVIATION LIST.....	X
<b>CHAPTER 1: THE USE OF 3D-PRINTING OF PATIENT-SPECIFIC GUIDES IN LUMBAR SPINE SURGERY – A SYSTEMATIC REVIEW.....</b>	<b>1</b>
INTRODUCTION.....	1
METHODS.....	5
RESULTS.....	7
<i>Figure 1</i> .....	8
DISCUSSION.....	9
<i>Table 1</i> .....	11
CONCLUSION.....	22
CHAPTER 1 REFERENCE LIST.....	22
<b>CHAPTER 2: GEOMETRIC AND VOLUMETRIC RELATIONSHIP BETWEEN HUMAN LUMBAR VERTEBRA AND CT BASED MODELS.....</b>	<b>27</b>
INTRODUCTION.....	27
METHODS.....	29
<i>Figure 1</i> .....	29
<i>Figure 2</i> .....	34
RESULTS.....	35
<i>Table 1</i> .....	37
<i>Table 2</i> .....	38
<i>Figure 3</i> .....	39
<i>Figure 4</i> .....	41
DISCUSSION.....	42
CONCLUSION.....	48
CHAPTER 2 REFERENCE LIST.....	48
<b>CHAPTER 3: THE DEVELOPMENT OF NOVEL 2-IN-1 PATIENT SPECIFIC, 3D-PRINTED LAMINECTOMY GUIDES WITH INTEGRATED PEDICLE SCREW DRILL GUIDES.....</b>	<b>52</b>
INTRODUCTION.....	52
<i>Figure 1</i> .....	55
METHODS.....	56
<i>Figure 2</i> .....	56
<i>Figure 3</i> .....	60



RESULTS .....	64
<i>Table 1</i> .....	64
DISCUSSION .....	66
CONCLUSION .....	73
CHAPTER 3 REFERENCE LIST .....	73
<b>CHAPTER 4: .....</b>	<b>77</b>
<b>(A) ERROR MEASUREMENT BETWEEN BLACK-BONE MRI-BASED AND CT-BASED MODELS;....</b>	<b>77</b>
<b>(B) THE DEVELOPMENT OF NOVEL 2-IN-1 PATIENT SPECIFIC, MRI-BASED 3D-PRINTED LAMINECTOMY GUIDES WITH INTEGRATED PEDICLE SCREW GUIDES.....</b>	<b>77</b>
INTRODUCTION .....	77
<i>Figure 1</i> .....	79
METHODS.....	80
<i>Figure 2</i> .....	80
<i>Table 1</i> .....	81
<i>Figure 3</i> .....	83
RESULTS .....	86
<i>Figure 4</i> .....	87
<i>Figure 5</i> .....	88
<i>Table 2</i> .....	89
DISCUSSION .....	91
CONCLUSION .....	97
CHAPTER 4 REFERENCE LIST .....	98
<b>APPENDIX.....</b>	<b>101</b>
ENGINEERING DRAWINGS.....	101
CURRICULUM VITAE.....	104

## Declaration of conflicting interests

The author has no potential conflicts of interest with respect to the research presented in this thesis.

## Funding

There has been no financial support for this research.

## Contributions

Andrew Kanawati – conceived ideas, experimental design, performed experiments, data collection, data analysis, and primary author.

Parham Rasoulinejad – supervisor, provided access to crucial research components, performed experiments, and provided revisions to scientific content of manuscript.

Chris Bailey – supervisor and provided access to crucial research components.

Aaron Gee – experimental design, performed experiments, data collection, provided revisions to scientific content of manuscript.

Renan Fernandes – performed experiments, data collection, data analysis, and provided revisions to scientific content of manuscript.

Jennifer Urquhart – data analysis and interpretation.

## Abbreviation list

3D	3-Dimensional
2D	2-dimensional
CT	Computed tomography
PSG	Patient-specific guide
STL	Standard tessellation language
DICOM	Digital imaging and communication in medicine
MRI	Magnetic resonance imaging

## Chapter 1: The use of 3D-printing of patient-specific guides in lumbar spine surgery – a systematic review

Key words:

Human spine.

Lumbar spine.

Image Processing, Computer-Assisted.

3D-printing.

Patient-specific guides.

Spine surgery.

Pedicle screw.

Spine instrumentation.

### Introduction

One of the commonest, yet most challenging aspects of spine surgery, is the insertion of screws into the vertebra. The pedicle is a channel of bone which connects of posterior neural arch structures to the anterior vertebral body. It is through this channel of bone where screws are inserted. These screws are termed 'pedicle screws'. There are several techniques which are in use the enable surgeons to insert pedicles screws, each with distinct advantages and disadvantages. The most traditional technique, called the 'freehand' technique, uses landmarks around the spine to assist insertion. This is the most cost-effective technique but has a high rate of screw misplacement (pedicle perforation). More advanced techniques to assist surgeons with pedicle screw insertion have reduced pedicle perforation rates but can involve high doses

of ionizing radiation and expensive equipment. Three-dimensional (3D)- printing is a promising technology which can assist surgeons in the insertion of pedicle screws. 3D-printing potentially has many of the advantages of the above techniques, and less of the disadvantages.

3D-printing refers to the manufacturing process in which a 3D digital model can be transformed into a physical model by layering material in the shape of successive cross sections atop of previously layers. Its use in the field of medicine, especially in spine surgery, has increased dramatically over the last ten years <sup>1</sup>. 3D-printing allows surgeons and physicians to personalize health care, using the patient's advanced medical imaging, such as computed-tomography (CT), to create patient-specific guides (PSGs). The main application of this in spinal surgery is the transfer of a carefully pre-planned screw position and size to a physical guide (also called jig or template). This guide exactly fits exactly to the unique anatomy of each individual patient, which theoretically increases precision. The main reported advantages of PSG include: low costs when compared to navigation platforms, minimal risk for patient and surgical team, reduced radiation exposure for surgical teams compared to navigation techniques, and improvements in precision and sizing of surgical instrumentation due to guide individualization <sup>2</sup>. Disadvantages of PSGs include errors in creating medical models, printing

Lumbar pedicle screw fixation is used throughout the world for treatment of spine trauma, degenerative conditions, scoliosis, tumors and infections <sup>3</sup>. Traditional methods of pedicle screw implantation include free-hand techniques or use of 2-dimensional (2D) intraoperative x-ray (fluoroscopy). More advanced techniques for pedicle screw implantation include

intraoperative navigation and robotic-assisted techniques. These advanced techniques have been introduced in order to increase screw placement accuracy and reduce pedicle perforation rates. Pedicle perforation increases risk of damage to anatomical structures adjacent to the pedicles, such as spinal cord, cauda equina, nerve roots and blood vessels <sup>4</sup>.

Free-hand techniques involve using anatomical landmarks and vertebral orientation to create the screw entry point and trajectory. This technique requires more extensive soft tissue dissection to visualize anatomy but is effective for appropriately trained surgeons.

Unfortunately, the free-hand technique has a high rate of unplanned pedicle perforation rate.

Complications of screw malposition include neural injury, dural tear, vascular injury and infection. Thoracic pedicle screw perforation rate ranges from 25% - 41% in some reports <sup>4,5</sup>.

Intraoperative x-ray use exposes the surgical team and patient to potentially large doses of radiation but allows for percutaneous surgery in select cases <sup>6</sup>. The rate of pedicle screw perforation using 2D fluoroscopy improves to 5.1% - 13.4% <sup>7</sup>.

Recent advances in intra-operative navigation systems have allowed for intraoperative 3D imaging acquisition and increased accuracy of instrumentation. The advantages of navigation systems are the most obvious when utilized on patients with more complex spinal anatomy, for example, scoliotic deformities <sup>8</sup>. Several weaknesses of these systems include: a significant learning curve; the optical array devices that can be obscured or shifted by surgical team members or instruments; and high cost. The overall reported rate of screw malposition of CT-

based navigation is 8.5% -11%<sup>9 10</sup>. High rates of malposition are due to mismatch of navigation and intraoperative position due to inter-segmentary vertebral movement during surgery or optical array shift. Intraoperative navigation requires registration of bone structures which takes varying amounts of time and require additional personnel during surgery. These additional factors lead to increase surgical time, and therefore, a higher theoretical risk of intraoperative infection<sup>11</sup>. Robotic systems use a similar integration of pre-operative or intra-operative CT scan to assist screw placement using a robotic arm capable of multiplanar mobility. Screw placement accuracy and complications are least comparable if not superior to freehand placement<sup>12</sup>.

Traditional free-hand techniques and more advanced methods, such as navigation, still play an important role in spine surgery; however, their deficiencies have led to continuing advances in other techniques, including the use of PSGs.

Several steps are involved in PSG production and are applicable across all medical fields. Many of the steps require collaboration between medical specialists and engineers, however several open source segmentation platforms are allowing non-engineering personal to create models and guides without significant learning curves or costs<sup>13</sup>. Examples of open source software are 3D Slicer ([www.slicer.org](http://www.slicer.org), Brigham and Women's Hospital, Boston, MA) and Osirix (Pixmeo, Geneva, Switzerland). The basic steps of the PSG production line include obtaining patient scan data, creating an anatomical model (segmentation), planning of surgical instrumentation,

creating surgical guides digitally, 3D-printing of the physical guides, and finally the sterilization and utilization of the guides.

Despite the several obvious advantages of PSGs in spine surgery, there are disadvantages unique to this technique. The sources of error include: learning curves associated with segmentation, manual and auto-segmentation errors, errors converting DICOM (digital imaging and communication in medicine) files to standard tessellation language (STL - the file format for 3D-printing) files, printing inaccuracies, improper guide placement due to interposed soft tissue, guide movement during surgical steps and the environmental impact of disposable guides <sup>1</sup>.

The purpose of this review is to assess the effectiveness PSGs in clinical lumbar spinal surgery. To this end, the aim of this systematic review is to identify clinical studies which utilize PSGs in lumbar spinal surgery, with a focus on those that have quantifiable outcomes. It should be noted that in this field, there are only short-term follow-up studies, which are most pertinent in that these techniques are mainly intraoperative aides that influence factors such as surgical times and surgical precision. Outcomes of these surgical procedures rely on a complex array of factors and use of PSGs as an independent factor would need large, well-designed cohorts to compare longer-term differences in clinical outcomes.

## Methods



The systematic review was performed according to the Preferred Reporting Items for Systematic Reviews and Meta-Analysis (PRISMA) guidelines. A search of MEDLINE and PubMed was performed, looking at English-language literature in the form of clinical trials and evaluation studies. The search period was limited to the ten-year period from 2009-2019.

Despite the use of PSG in lumbar spine surgery dating back to 1997 when Van Brussel et al. used the first drill template for the insertion of pedicle screws<sup>14</sup>, 2009 marks the point of patent expiration for fused deposition modeling (FDM), another common technique used for 3D-printing. This, and several other factors, lead to a substantial increase in interest of 3D-printing in medicine, therefore the search was limited to 2009-2019 as a more specific time period<sup>1</sup>.

Search terms included: pedicle screw, patient specific guide, 3D-printing, template, lumbar spine, orthopedic instrumentation, and computer-aided surgery as either key words or MeSH terms.

Inclusion criteria were established before the search, and studies meeting all the following conditions were eligible: (1) clinical study examining comparison between PSGs and free-hand techniques, or well-designed studies examining PSGs techniques only; (2) insertion of lumbar pedicle screws; and (3) a post-operative CT scan used to assess for pedicle breach, and/or angular difference. Exclusion criteria were as follows: (1) incomplete data; (2) cadaveric study; (3) non-English publication; and (4) duplicate publication.

## Results

After applying the primary search strategy, 271 articles were selected. After exclusion of articles based on title and abstract, 25 articles were selected for detailed examination. After review of the full text articles, 7 studies were selected for final review ([Figure 1](#)).

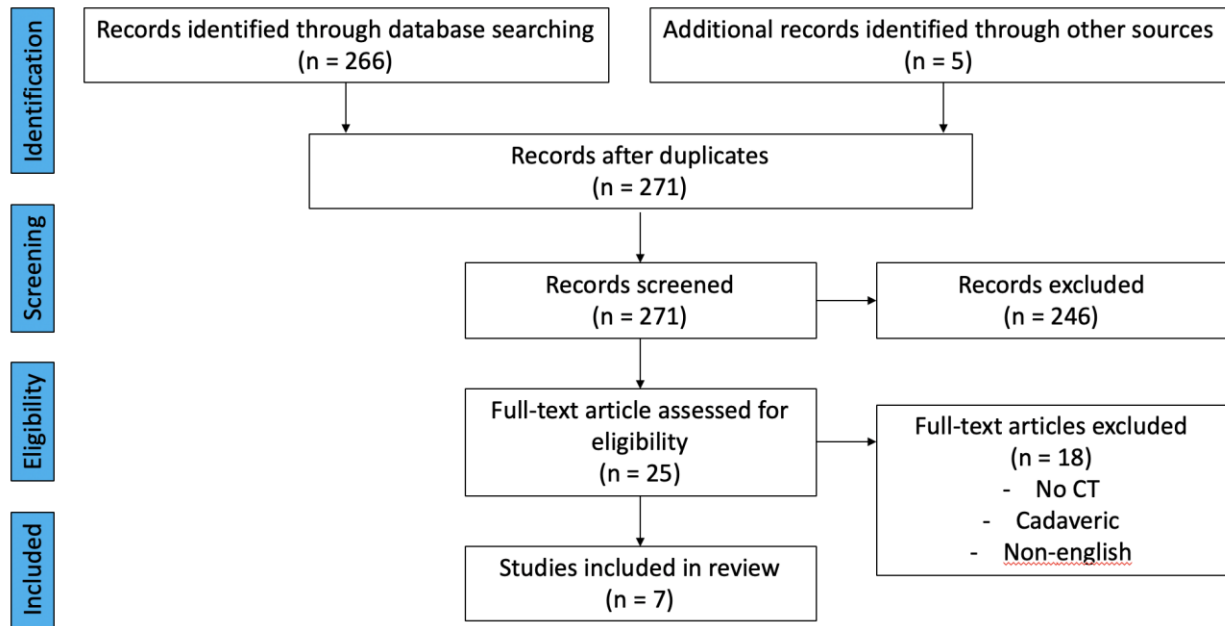


Figure 1

PRISMA flowchart for systemic review of clinical use of 3D-printing of PSGs in lumbar spine surgery.

All the included studies were retrospective in design, and all except one were immediate postoperative follow-up assessments. Only one study included intermediate (3 year) follow up

15.

In total, 362 lumbar pedicle screws were inserted using PSGs. 23 screws caused cortical breach on postoperative CT scans, with an average breach rate of 6% (range 0 – 18% breach rate).

The primary discussion will be focused on lumbar pedicle screw accuracy since this was the primary outcome of most investigations. Secondary discussion points pertinent to PSGs are also discussed. These issues include cost of PSGs compared to other screw insertion techniques, patient-safety relating to radiation exposure and use of potential toxic materials, production time, and PSG design considerations.

## Discussion

In 2009 the patent of FDM process expired, which led to an increased interest in 3D-printing in many different fields. However, since stereolithography (SL) is the form of 3D-printing in medicine, it is thought that the publicity surrounding 3D-printing had a greater impact on its use, rather than the expiration of the FDM patent per se. The availability of relatively inexpensive desktop 3D-printers and overall decrease in cost of parts has also guided the increase in use of 3D-printing in medicine <sup>1</sup>.

Popescu et al. performed a systematic review of PSGs in general orthopedic and orthopedic spinal surgery. Most of the applications of PSG in medicine are used in spinal orthopedic surgery. Using PSGs removes the requirements for complex equipment and time-consuming procedures in the operating suite. Additionally, PSGs are a simple, low-cost technique that generates patient-specific and bone-specific tools <sup>1</sup>.

In all of the papers reviewed, several advantages of PSG can be identified: (1) improved surgical accuracy when compared to free-hand techniques ([Table 1](#)); (2) reduced cost compared to navigation and robotics platforms; (3) reduced radiation for surgical teams; and (4) rapid turnover.

Study (name/year)	Country	Participants	Condition	Interventions (patients/screws)	Pedicle screw accuracy or cortical perforation rate
<b>Merc 2017</b> <sup>15</sup>	Slovenia	24	Degenerative lumbar	PSG 11 patients, 72 screws. FH – 13 patients, 72 screws.	Cortical perforation rates: PSG - 8.3 % (6/72) FH – 40 % (29/72)
<b>Putzier 2017</b> <sup>8</sup>	Germany	4	Scoliosis	PSG – 20 lumbar screws	PSG – 16 % (3/20)
<b>Otsuki 2016</b> <sup>20</sup>	Japan	5	Revision cervical (1) / lumbar (2)	PSG – 4 lumbar screws	PSG – 0 % (0/4)
<b>Chen 2015</b> <sup>19</sup>	China	43	Degenerative lumbar	PSG – 20 patients, 118 screws FH – 23 patients, 122 screws	PSG – 8.5 % breach (10/118) FH – 17.2 % breach (21/122)
<b>Merc 2014</b> <sup>17</sup>	Slovenia	11	Degenerative lumbar	PSG – 11 patients, 72 screws	PSG – 0 % (0/72)
<b>Merc 2013</b> <sup>16</sup>	Slovenia	20	Degenerative lumbar	PSG – 9 patients, 54 screws. FH – 10 patients, 54 screws	PSG – 7 % (4/54) FH – 17 % breach (9/54)
<b>Lu 2009</b> <sup>18</sup>	China	6	Not specified	PSG –6 patients, 22 screws	PSG – 0 % (0/22)

Table 1

Description of screw accuracy for included studies. PSG – patient-specific guide, FH – free-hand.

Improved accuracy (Table 1):

In all the studies reviewed, screw accuracy for PSGs was equal to or better than free-hand techniques, with overall accuracy rates ranging between 84% - 100%, and an average breach rate of 6% (23 of 362 screws). These rates of screw accuracy are for lumbar spine screw insertion only. In a systematic review of 26 clinical studies examining pedicle screw accuracy in the thoracic and lumbar spines, the rates of screws without breach were reported to range from 69% to 94% for free-hand placement, compared to 25% to 85% with fluoroscopy, and 89% to 100% with navigation <sup>10</sup>. No studies were identified directly comparing PSGs to navigation or robotic-assisted techniques.

Merc et al. compared multi-level lumbar PSGs in 9 patients, to 10 patients in a free-hand group with 54 screws inserted in each group <sup>16</sup>. Post-operative CT scans showed significantly lower cortical perforation in the PSGs group versus free-hand group, 7% versus 17% respectively. This was the first study to examine sacral pedicle screw PSGs. Their major criticism of PSGs was the need to strip large areas of soft tissue from the bone, to ensure a good fit to the dorsal spinal elements. Furthermore, the investigators needed to perform pre-operative CT scans with the patients lying in the prone position to simulate similar facet joint relations as the intra-operative prone position. There has been no standardization of PSGs with regards to design geometry, number of levels of use and position of the patient when scans are performed.

Merc et al.<sup>17</sup> performed a case series on 11 patients and inserted 72 screws using multi-level PSGs. They did not report any pedicle violations, however 26% of the screws were implanted inaccurately compared to the pre-planned trajectory. They concluded that multi-level PSGs have a perceivable but acceptable error rate, and if these guides were subjected to improved designs, they might be a successful solution for spinal surgery applications.

Merc et al. performed the first intermediate-term clinical follow-up of 11 patients in the PSG group, and 13 in a freehand control group<sup>15</sup> (follow-up of the patients in the above study). 72 screws were inserted in each group. The rate of cortical perforation was significantly lower in the PSG group 6/72 (8.3%) versus the control group 29/72 (40%). Both groups had a significant decrease in back and leg pain, and disability scores, however there was no statistical difference between each group for these measures at 3 years follow-up. They did not measure or compare intra-operative parameters such as operative time, fluoroscopy time and blood loss. They concluded that although PSGs result in more accurate screw placement, it does not influence the intermediate pain and disability outcomes of the procedure.

Lu et al.<sup>18</sup> performed a cadaveric, and then clinical case series, on thoracic and lumbar spines. They inserted 22 screws in six patients, with no screw misplacement. The authors claimed radiation exposures for the surgical team were significantly reduced,



however exact surgical times, screw trajectory comparisons and fluoroscopy times were not noted. Stripping of the soft tissues to ensure satisfactory contact between the bone and template was again noted as a draw-back of the PSG technique. However, use of PSGs requires less exposure of the transverse processes, therefore it is likely the overall soft tissue damage is equal compared to conventional techniques.

Chen et al.<sup>19</sup> used PSGs in 20 patients and compared them to FREEHAND screw insertion in 23 patients. A total of 118 screws were inserted in the PSG group, compared to 122 screws in the control group. The mean time of placement for each screw was 4.9 +/- 2.1 mins in the experimental group, and 6.5 +/- 2.2 mins in the control group. The accuracy of screw placement was excellent and good in 91.5% and 8.5% respectively in the PSG group, compared to 81.1% and 17.2% respectively in the control group. They conclude that PSGs improved operative times and screw placement accuracy.

Putzier et al.<sup>8</sup> implanted 76 pedicle screws using PSGs (56 thoracic, 20 lumbar) in 4 patients with severe scoliosis. Overall, 84% of the pedicle screws were completely intra-pedicular, and 96.1% were within <2mm cortical breach. All lumbar screws were intra-pedicular. No medial pedicle breeches were detected on CT, and no-screw related clinical complications were reported postoperatively. Two screws (2.6%) were intraoperatively repositioned. Only the lumbar screws were included in analysis of screws in this review. They believe that their technique had a very short learning curve and has the potential to be easily adopted.

Otsuki et al.<sup>20</sup> were the first to use PSGs in revision spine surgery. 5 screws in 3 patients (1 cervical and 2 lumbar) were inserted using titanium powder based PSGs that were printed using selective laser-melting technique. Only the lumbar screws were included in analysis of screws in this review. The guides had 5 – 6 small arms that were carefully selected to contact areas with relatively high CT contrast values. All screws were positioned successfully. Authors cite several advantages using PSG in revision surgery: (1) ability to digitally remove implants from previous surgery; (2) intraoperative availability of the 3D printed bio-model allowed safe surgical exposure through scar tissue around complex bone shapes; (3) screw insertion with PSGs required only ‘a few minutes’ in each case; and (4) time saving compared to navigation techniques. The cumulative time taken to segment, print and use the PSGs was not examined.

#### Reduced cost:

The 3D-printing process is more affordable in terms of start-up setup and ongoing costs, compared to computer-assisted navigation or robotic-assisted systems. All of these advanced techniques, PSGs and navigation alike, have been shown to reduce instrumentation errors and improve surgical times.

The current cost of a Formlabs Form 2 (Formlabs Inc. Somerville, MA) desktop 3d-printer is US\$3850. This 3D-printer is capable of printing any spinal model and PSG

within a print volume of 145 x 145 x 175mm. Assuming the use of the Formlabs 3D printer and Surgical Guide Resin, the approximate manufacturing cost of PSGs is US\$20-50 per level<sup>9,21,22</sup>. The labor costs of an engineer need to be taken into account, since it can take up to 2 hours to create and prepare bio-models and PSGs per level. Furthermore, FDA-approved software costs and the initial cost of bringing this technology to market and passing regulatory requirements would result in significantly higher costs than those of manufacturing alone. Therefore, despite the cost of printing and materials decreasing significantly in recent years, the start-up costs of equipment and full-time staff should be considered. If PSGs production is outsourced to a private company, instead of using in-house printers and software, a single guide can cost up to US \$500 to produce.

The average price for the Medtronic O-arm Imaging System without the navigation interface is US\$682,000<sup>23</sup>. The estimated life cycle of the system is 8 to 10 years. The average price of a computer-assisted navigation interface that can be used with the O-arm Imaging System is US\$265,000. Only Medtronic screw systems are recommended to be used with the O-arm imaging system which can be a problem for some institutions that do not use Medtronic equipment, although other navigation platforms exist that do not require proprietary implants. The labor costs of a radiographer required for the operation of these systems must also be taken into account<sup>23</sup> Service schedules are expensive, accounting for approximately US\$50,000 annually. Navigation platforms also require space inside and outside the operating room, which is often restrictive.

Furthermore, during the learning curve, the navigation procedure can be fault-prone and time consuming <sup>24</sup>.

Renaissance (Mazor Robotics, Caesarea, Israel) is a widely used spinal robotic system, and costs approximately US\$400,000 to \$850,000, with disposable costs of approximately US\$2000 per case. Currently these new robotic arm platforms require more clinical and health economic data to rationalize their increased costs, as their results and complications appear to be similar to other techniques <sup>12 23</sup>.

#### Radiation exposure and other patient safety issues:

The use of PSGs in the lumbar spine requires the acquisition of one pre-operative CT scan of the lumbar spine. This exposes only the patient to radiation, but spares exposure to the surgical team. Use of intra-operative navigation may expose the patient and surgical team to radiation, however surgical teams are encouraged to leave the theatre during the scanning process, or wear adequate radiation protection including lead glasses and gowns <sup>23</sup>. For interests' sake, doses of both thoracic and lumbar CT scans have been included in the discussion.

Richards et al. described the estimated dose of a pre-operative CT lumbar spine to be about 5.6 mSv (560uSv) with an estimated cancer risk of 1 in 3,200, compared to a typical chest radiograph estimated effective dose of 0.02 mSv (20uSv), which gives a

relative risk of causing cancer of about 1 in 1,000,000 <sup>25</sup>. CT scans of the Thoracic spine may result in even higher doses of radiation exposure. Zhang et al. measured organ absorbed dose on a phantom undergoing a routine adult chest CT, which ranged from 9.4 to 18.8 mGy <sup>26</sup>.

Pitteloud et al. described the radiation exposure of patients and staff using the O-arm surgical system using anthropomorphic phantoms <sup>6</sup>. Patient organ doses ranged from 30 +/- 4 uGy to 20 +/- 3.0 mGy and 4 +/- 1 uGy to 6.7 +/- 1.0 mGy for a 3D thoracic spine and pelvic examination, respectively. For a single 3D acquisition, the maximum ambient dose (for staff) at 2m from the isocenter was 11 +/- 1 uSv. Therefore, patients are almost equivalently irradiated using conventional CT scans. However, in some circumstances, such as thoraco-lumbar fusions for scoliosis, two O-arm sequences are used (one for the thoracic screws, and one for lumbar/thoraco-lumbar screws). Therefore, every O-arm sequence should be carefully considered, as cumulative exposure may be significant. Still, a major limitation of the PSG production is the need to obtain a preoperative CT scan, thus exposing the patient to radiation.

All of the studies examined in this review utilize CT scans to acquire the DICOM information to create 3D bio-models. CT scan protocols included 0.625mm slice thickness, and 0.35mm in-plane resolution.

No studies have used MRI to create spine bio-models, as MRI is still not precise enough for 3D reconstruction due to too much information at the bone-soft tissue interface <sup>1</sup>.

Another patient safety concern is potential toxicity of the surgical guide material when in contact with human tissue. Some animal models have reported toxic effects of 3D-printed parts <sup>27</sup>, however there have been no reports of any toxic effects in humans.

Several approaches exist to prevent drilling and saw related debris, including insertion of metal inserts in the plastic guides, or use of biocompatible guides. Formlabs (Formlabs Inc. Somerville, MA) introduced a Surgical Guide resin in 2019 which is biocompatible and meets Class I requirements. After being post-cured, this material can be chemically disinfected, or steam sterilized in an autoclave. This resin has been classified as non-cytotoxic, non-irritant and not a sensitizer <sup>28</sup>.

#### Rapid turnover time:

Improvements in converting medical imaging into bio-models and 3D-printing technologies has meant that PSGs can be produced with relatively fast turn-over times. Sugawara et al. describes 2-3 days for the entire production line, with 1-2 days of design, and then 1 day for printing and post-processing <sup>9</sup>. This would certainly be the case if PSGs used for scoliosis correction where more than 3-4 levels of instrumentation are required. However, it has been our experience that up to 4 lumbar drill guides and bio-models can be produced in a single print, which takes approximately 7-8 hours to

print. Therefore, it is feasible that a patient who needs semi-urgent surgery, could have a CT scan one day and PSGs could be designed, printed and sterilized for surgery the next day, if the 3D-printer was left to print overnight. This was confirmed by Lu et al. who described a PSG manufacture time of 16 hours per patient <sup>22</sup>.

### PSG design considerations:

Putzier et al. <sup>8</sup> describes the ideal features of a PSG through their cadaveric and then clinical study. An optimal design should guarantee stability, screw position accuracy, with minimal invasiveness which is simple and reproducible. The ideal design should have the following features: (1) guides created for each vertebra separately should avoid contact with adjacent levels caused by inter-segmentary movement differences between the supine imaging position and the prone surgical position; (2) each step in the PSG operative process should be possible while maintaining surgical goals of traditional open procedures; (3) contact points have to offer a balance between stability and tactile feedback during drilling; (4) bone contact points should be positioned in areas typically exposed during a traditional open approach; and (5) the guide should offer satisfactory visual verification of accurate attachment.

Despite the versatility of use and variations of designs, there has been a lack of growth in other applications of PSGs in spinal surgery, such as guides for complex osteotomy (such as pedicle subtraction osteotomy), or guides to assist in laminectomy.

### Limitations of PSGs:

Several disadvantages exist when using PSGs, with most stemming from inaccuracies that arise during the production line. PSGs are complex in design and guide surgical instruments, and sometimes power tools. They need to be easily positioned and keep their position during use. Another important feature is to allow the operator to check their position during use, by windows in the guide or by using transparent material <sup>1</sup>.

Sources of error can begin when acquiring the medical imaging (CT scan). This can occur if image slices are not thin enough (usually 0.625mm thickness is necessary), or if motion and metal artefacts are present. These errors will lead to inaccuracies when data is transferred from DICOM to STL (the file format for 3D-printing) files.

PSGs are modelled as a template of the anatomical structure, usually the lamina, facet joints, and spinous or transverse processes. If the bio-model created from the DICOM data is not accurate, then any PSG created will not fit on the bone properly or not be accurate. Insufficient removal of soft tissues in the regions where the guide needs to be placed can lead to inaccuracies in screw placement.

A learning curve exists when any new technique is introduced, however this learning curve has not been formally assessed in any studies. Ma et al. state that the learning



curve needed for PSGs is less than that needed for free-hand, navigation or robotic-assisted techniques <sup>29</sup>.

The 3D-printing production line requires specific knowledge regarding design and manufacture of PSGs. This requires collaboration between engineers and surgeons. Breakdown in communication or poor surgical planning can lead to obvious inaccuracies, which can occur when transferring knowledge of medical requirements into processes of design, choice of material and manufacturing of physical objects <sup>1</sup>.

## Conclusion

3D-printing is an ever-expanding field in medicine, and production of PSGs is becoming more popular due to multiple benefits, including increased accuracy, affordability, safety of use, and rapid turn-over times. This review has highlighted and summarized the usefulness of PSGs in clinical lumbar spine surgery. The availability of relatively affordable desktop 3D-printers and several open-source segmentation software programs are reducing the inter-disciplinary barriers to the use of PSGs. Further exciting work in this area will include guides for complex osteotomy and laminectomy, and the use of non-ionizing imaging to create bio-models and guides. More research will be necessary, in the form of large clinical trials or case-control series, to determine if there are any long-term clinical differences in outcomes when using PSG.

## Chapter 1 Reference list

1. Popescu D, Laptoiu D. Rapid prototyping for patient-specific surgical orthopaedics guides: A systematic literature review. *Proc Inst Mech Eng H*. 2016;230(6):495-515.  
doi:10.1177/0954411916636919
2. Cecchinato R, Berjano P, Zerbi A, Damilano M, Redaelli A, Lamartina C. Pedicle screw insertion with patient-specific 3D-printed guides based on low-dose CT scan is more accurate than free-hand technique in spine deformity patients: a prospective, randomized clinical trial. *Eur Spine J*. 2019;28(7):1712-1723. doi:10.1007/s00586-019-05978-3
3. Belmont PJ, Klemme WR, Robinson M, Polly DW. Accuracy of thoracic pedicle screws in patients with and without coronal plane spinal deformities. *Spine*. 2002;27(14):1558-1566.  
doi:10.1097/00007632-200207150-00015
4. Castro WH, Halm H, Jerosch J, Malms J, Steinbeck J, Blasius S. Accuracy of pedicle screw placement in lumbar vertebrae. *Spine*. 1996;21(11):1320-1324. doi:10.1097/00007632-199606010-00008
5. Vaccaro AR, Garfin SR. Internal fixation (pedicle screw fixation) for fusions of the lumbar spine. *Spine*. 1995;20(24 Suppl):157S-165S.
6. Pitteloud N, Gamulin A, Barea C, Damet J, Racloz G, Sans-Merce M. Radiation exposure using the O-arm® surgical imaging system. *Eur Spine J*. 2017;26(3):651-657.  
doi:10.1007/s00586-016-4773-0
7. Oh HS, Kim J-S, Lee S-H, Liu WC, Hong S-W. Comparison between the accuracy of percutaneous and open pedicle screw fixations in lumbosacral fusion. *Spine J*. 2013;13(12):1751-1757. doi:10.1016/j.spinee.2013.03.042

8. Putzier M, Strube P, Cecchinato R, Lamartina C, Hoff EK. A New Navigational Tool for Pedicle Screw Placement in Patients With Severe Scoliosis: A Pilot Study to Prove Feasibility, Accuracy, and Identify Operative Challenges. *Clin Spine Surg.* 2017;30(4):E430-E439. doi:10.1097/BSD.0000000000000220
9. Sugawara T, Higashiyama N, Kaneyama S, et al. Multistep pedicle screw insertion procedure with patient-specific lamina fit-and-lock templates for the thoracic spine: clinical article. *J Neurosurg Spine.* 2013;19(2):185-190. doi:10.3171/2013.4.SPINE121059
10. Gelalis ID, Paschos NK, Pakos EE, et al. Accuracy of pedicle screw placement: a systematic review of prospective in vivo studies comparing free hand, fluoroscopy guidance and navigation techniques. *Eur Spine J.* 2012;21(2):247-255. doi:10.1007/s00586-011-2011-3
11. Hughes SP, Anderson FM. Infection in the operating room. *J Bone Joint Surg Br.* 1999;81(5):754-755. doi:10.1302/0301-620x.81b5.10370
12. Ghasem A, Sharma A, Greif DN, Alam M, Maaieh MA. The Arrival of Robotics in Spine Surgery: A Review of the Literature. *SPINE.* 2018;43(23):1670-1677. doi:10.1097/BRS.00000000000002695
13. Ripley B, Levin D, Kelil T, et al. 3D printing from MRI Data: Harnessing strengths and minimizing weaknesses. *J Magn Reson Imaging.* 2017;45(3):635-645. doi:10.1002/jmri.25526
14. Van Brussel, K, Sloten JV, Van Audekercke R, B Swaelens, F Richard. Medical image based design of an individualized surgical guide for pedicle screw insertion. November 1996.
15. Merc M, Recnik G, Krajnc Z. Lumbar and sacral pedicle screw placement using a template does not improve the midterm pain and disability outcome in comparison with free-

hand method. *Eur J Orthop Surg Traumatol*. 2017;27(5):583-589. doi:10.1007/s00590-017-1904-1

16. Merc M, Drstvensek I, Vogrin M, Brajliah T, Recnik G. A multi-level rapid prototyping drill guide template reduces the perforation risk of pedicle screw placement in the lumbar and sacral spine. *Arch Orthop Trauma Surg*. 2013;133(7):893-899. doi:10.1007/s00402-013-1755-0

17. Merc M, Drstvensek I, Vogrin M, Brajliah T, Friedrich T, Recnik G. Error rate of multi-level rapid prototyping trajectories for pedicle screw placement in lumbar and sacral spine. *Chin J Traumatol*. 2014;17(5):261-266.

18. Lu S, Xu Y-Q, Zhang Y-Z, et al. Rapid prototyping drill guide template for lumbar pedicle screw placement. *Chin J Traumatol*. 2009;12(3):177-180.

19. Chen H, Wu D, Yang H, Guo K. Clinical Use of 3D Printing Guide Plate in Posterior Lumbar Pedicle Screw Fixation. *Med Sci Monit*. 2015;21:3948-3954. doi:10.12659/msm.895597

20. Otsuki B, Takemoto M, Fujibayashi S, Kimura H, Masamoto K, Matsuda S. Utility of a custom screw insertion guide and a full-scale, color-coded 3D plaster model for guiding safe surgical exposure and screw insertion during spine revision surgery. *J Neurosurg Spine*. 2016;25(1):94-102. doi:10.3171/2015.12.SPINE15678

21. Owen BD, Christensen GE, Reinhardt JM, Ryken TC. Rapid prototype patient-specific drill template for cervical pedicle screw placement. *Comput Aided Surg*. 2007;12(5):303-308. doi:10.3109/10929080701662826

22. Lu S, Xu YQ, Lu WW, et al. A novel patient-specific navigational template for cervical pedicle screw placement. *Spine (Phila Pa 1976)*. 2009;34(26):E959-966. doi:10.1097/BRS.0b013e3181c09985

23. Malham GM, Wells-Quinn T. What should my hospital buy next?-Guidelines for the acquisition and application of imaging, navigation, and robotics for spine surgery. *J Spine Surg.* 2019;5(1):155-165. doi:10.21037/jss.2019.02.04
24. Rivkin MA, Yocom SS. Thoracolumbar instrumentation with CT-guided navigation (O-arm) in 270 consecutive patients: accuracy rates and lessons learned. *Neurosurg Focus.* 2014;36(3):E7. doi:10.3171/2014.1.FOCUS13499
25. Richards PJ, George J, Metelko M, Brown M. Spine computed tomography doses and cancer induction. *Spine.* 2010;35(4):430-433. doi:10.1097/BRS.0b013e3181cdde47
26. Zhang D, Li X, Gao Y, Xu XG, Liu B. A method to acquire CT organ dose map using OSL dosimeters and ATOM anthropomorphic phantoms. *Med Phys.* 2013;40(8):081918. doi:10.1118/1.4816299
27. de Almeida Monteiro Melo Ferraz M, Henning HHW, Ferreira da Costa P, et al. Potential Health and Environmental Risks of Three-Dimensional Engineered Polymers. *Environ Sci Technol Lett.* 2018;5(2):80-85. doi:10.1021/acs.estlett.7b00495
28. <https://Dental.Formlabs.Com/Indications/Surgical-Guides/Guide/>.
29. Ma T, Xu Y-Q, Cheng Y-B, et al. A novel computer-assisted drill guide template for thoracic pedicle screw placement: a cadaveric study. *Arch Orthop Trauma Surg.* 2012;132(1):65-72. doi:10.1007/s00402-011-1383-5

## Chapter 2: Geometric and volumetric relationship between human lumbar vertebra and CT based models

Key words:

Human spine.

Lumbar spine.

Anthropometry.

Image Processing, Computer-Assisted.

Laser scanning.

CT.

3D-printing.

Anatomical models.

### Introduction

Several steps are involved in the 3D printing process, which include image acquisition, segmentation and creation of mesh models, postprocessing and the actual print process itself <sup>1</sup>.

Crucial to this process is the knowledge of how the actual structure or organ relates dimensionally to its corresponding medical image. Despite several studies examining the accuracy of 3D printed models to the corresponding computed topographic (CT) measurements, there is a paucity of evidence validating the accuracy of 3D models, when compared to the actual structure that has been imaged.

Brouwers et al. studied the difference between two measured points on cadaver pelvises, hands and feet. They compared the cadaver bones to 2-dimensional (2D), 3D models and 3D-printed models and found the most significant difference in measurements when converting the 3D file to the 3D printed model <sup>2</sup>. Most of their measurements between models were within 1mm differences. Reddy et al. found there was minimal difference between measurements on dry bones and 3D printed bone model, when examining bones of the appendicular skeleton <sup>3</sup>.

Several studies have confirmed the accuracy between CT measurements and the 3D printed models. Wu et al. examined 45 spine CTs and found that 88.6% of the parameters of cervical vertebrae, 90% of thoracic vertebrae and 94% of lumbar vertebrae had an intraclass correlation coefficient (ICC) values of >0.800 between radiographic images and 3D printed spine models <sup>4</sup>.

Galvez et al. studied the difference between 10 porcine lumbar spinal vertebra and CT images, as well as 3D printed models of these vertebra <sup>5</sup>. When compared to 3D printed models, there was an average error of 0.6mm with CT images, and 0.73mm with the anatomical piece. They concluded that 3D printed models accurately reflect porcine bones.

To our knowledge there are no human studies in the published literature that compare the characteristics of spinal bones to their corresponding CT measurements or 3D-printed models. This study will examine the differences between human lumbar vertebrae, 3D models based on CT scans, and 3D printed models.

## Methods

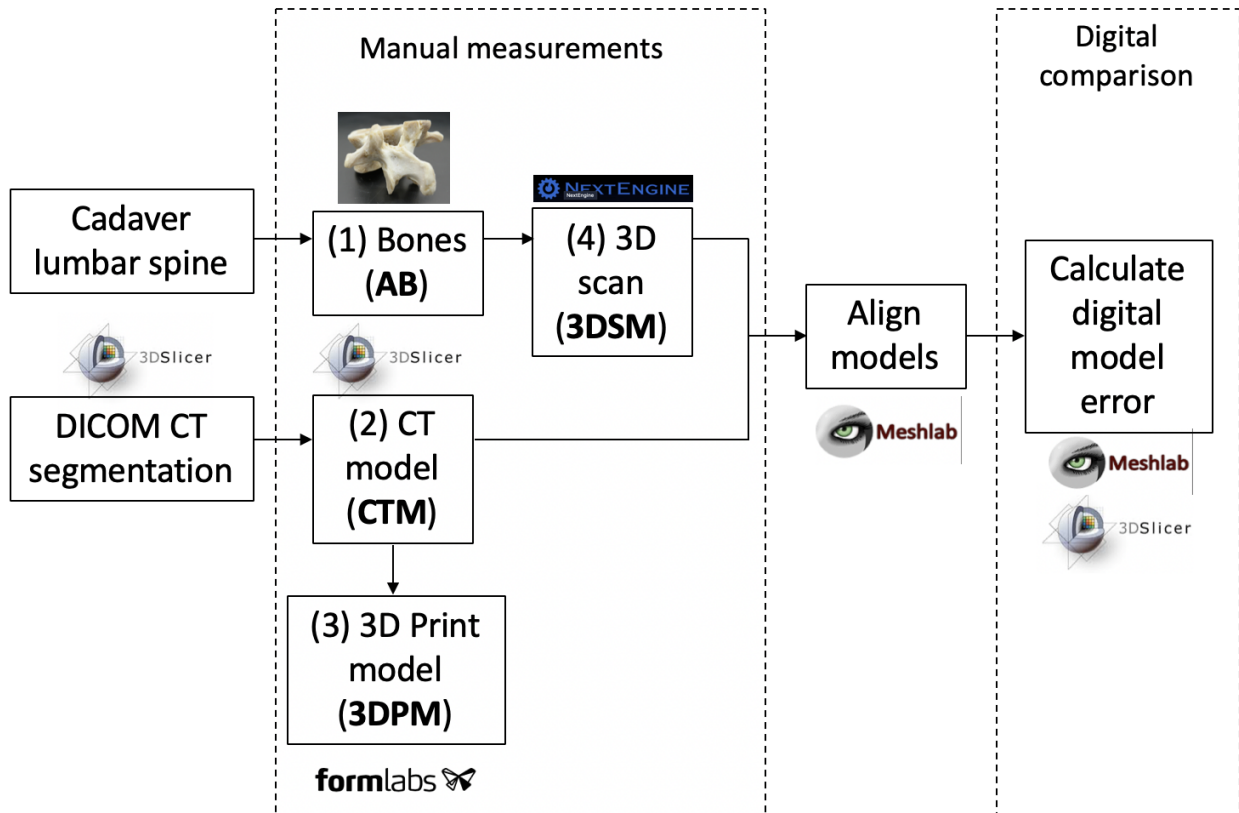


Figure 1

The workflow for comparing the 4 model types and obtaining manual and digital comparisons.

### Medical imaging:

After institutional ethics approval, six whole cadaver spines were harvested. The soft tissues, including the paraspinal muscles circumferentially, were left intact during the scanning processes, in order to replicate the clinical scenario as much as possible. The spines were scanned using GE Lightspeed VCT 64 slice CT Scanner with 0.625mm slicer thickness ([Figure 1](#)).

Details of the lumbar spine scanning protocol in our institution are as follows: Pitch 0.984:1,



table speed 39.37mm/ro, Helical Full 1.0s, SFOV: Large Body, DFOV 40 adjust as needed, 120 kVp, Auto mA: ON Smart mA: ON, Min mA: 200 Max mA: 650, Dose Reduction: 20%, Noise Index: 26 and ASIR: 40%.

#### Soft tissue removal:

The spines were isolated from T12 to sacrum, and were prepared in a similar fashion as described by Galvez et al. <sup>5</sup>. The bones were boiled, for 5 hours with dishwashing detergent, to make the process of cleaning much more efficient. The use of detergent facilitated the breakdown of fats and other tissues. After the boiling process, the specimens were meticulously cleaned in order to not inadvertently damage or distort the bones. A combination of gentle sharp dissection with no. 10 blades, curettes and periosteal elevators were used to remove soft tissue. The bones were designated as anatomic bones (AB) ([Figure 1](#)).

#### Digitization of bones:

The prepared bones were 3D scanned individually using a Next Engine <sup>TM</sup> 3D Scanner Ultra UH (Next Engine Inc, California), which uses multiple lasers to scan the surfaces of objects. A 20mm sphere test object was scanned and measured to ensure calibration. Due to the complex shape of the individual vertebra, 3 to 4 sets of 3D scans, with the bone oriented in different planes, were obtained to ensure all areas of the vertebra were scanned. The scans in different planes

were aligned and fused using Next Engine Scan Studio software, and a STL file was created. The digitized 3D scanned models were designated as 3DSM ([Figure 1](#)).

#### Images processing and segmentation metrics acquisition:

3D mesh models were created by importing the CT digital imaging and communication in medicine (DICOM) files into 3D Slicer version 4.10.2 ([www.slicer.org](http://www.slicer.org)).

A region of interest was created around each individual vertebra in question, with a crop scale of 0.5 and isotropic spacing. Cropping and resampling the volume before starting segmentation changes the segmentation node's internal binary label map and increases the resolution of subsequent models. Each vertebral model was created by using the semi-automated 'grow from seeds' extension in the Segment Editor of Slicer. Segmentation defects were corrected by modifying seeds and manual editing to ensure accuracy of the models. Closing (fills holes) and opening (remove extrusions) smoothing effects at a kernel size of 2mm were used to obtain a final model, which was exported as an STL file. The CT scan models were designated as CTM ([Figure 1](#)).

The 3DSM and CTM STL files were imported into Meshlab (v. 1.3.2, Consiglio Nazionale delle Ricerche – CNR, Rome, Italy), and aligned using an iterative closest point algorithm (point based gluing tool). At least 3 fiducial points were used to ensure the models were aligned appropriately. The aligned models were imported into 3D Slicer, and digital similarities between

the models were calculated using Hausdorff distance and Dice Coefficient, and segmentation volumes.

The Dice Coefficient, also called the overlap index, is a measurement of 3D overlap (in percentage) between segmented object and the ground truth (the segmentation performed manually by an expert). It is the most used metric in validating medical volume segmentations<sup>16</sup>. The Dice Coefficient ranges from 0, indicating no spatial overlap between two segmentations; to 1, indicating complete overlap. The literature on image validation indicates that good overlap occurs when the Dice Coefficient is  $>0.70$ <sup>18</sup>.

Hausdorff distance is a shape dissimilarity tool measuring the most mismatched points between the segmented object and the ground truth, expressed as the largest deviation of the boundaries from one another<sup>16</sup>. The Hausdorff distance is generally sensitive to outliers, which can be caused by noise and artefacts in medical segmentations. Therefore, the average Hausdorff distance is known to be more stable and less sensitive to outliers. High Dice Coefficients and low Hausdorff distance values indicate high accuracy of the image segmentation method.

### 3D printing:

CTM STL files were imported into Formlabs Preform software. The models were manually oriented on the build platform to avoid placing supports on parts of the model that would be measured. Supports were then automatically generated, but could be modified to

optimize contact points. Layer thickness was set to 0.1mm and printed in Grey resin. The 3D printed models were designated as 3DPM ([Figure 1](#)).

### Measurements:

The following 4 model types were compared: (1) AB, (2) 3DSM, (3) CTM, and (4) 3DPM.

To assess the accuracy of each method fifteen measurements were recorded for all model types ([Figure 2](#)). Bones that were damaged during the harvesting and cleaning process were excluded from manual measurement and 3D scanning analysis. Transverse processes that were obviously damaged during the cleaning process were also excluded from manual measurements. An Igaging EzCal fraction digital caliper, with 0.01mm resolution and 0.03mm accuracy, was used to make all manual measurements on the AB and 3DPM. Measurements were rounded to the nearest 0.1mm. The same parameters were recorded virtually for the 3DSM and CTM, using the virtual ruler tool in 3D slicer. Two spine surgeons recorded measurements of each model, blinded to knowledge of each other's measurements, and blinded to the measurements of other models of the same bone. Measurements were made on two different occasions of each models and averages of these measurements were made for statistical analysis.

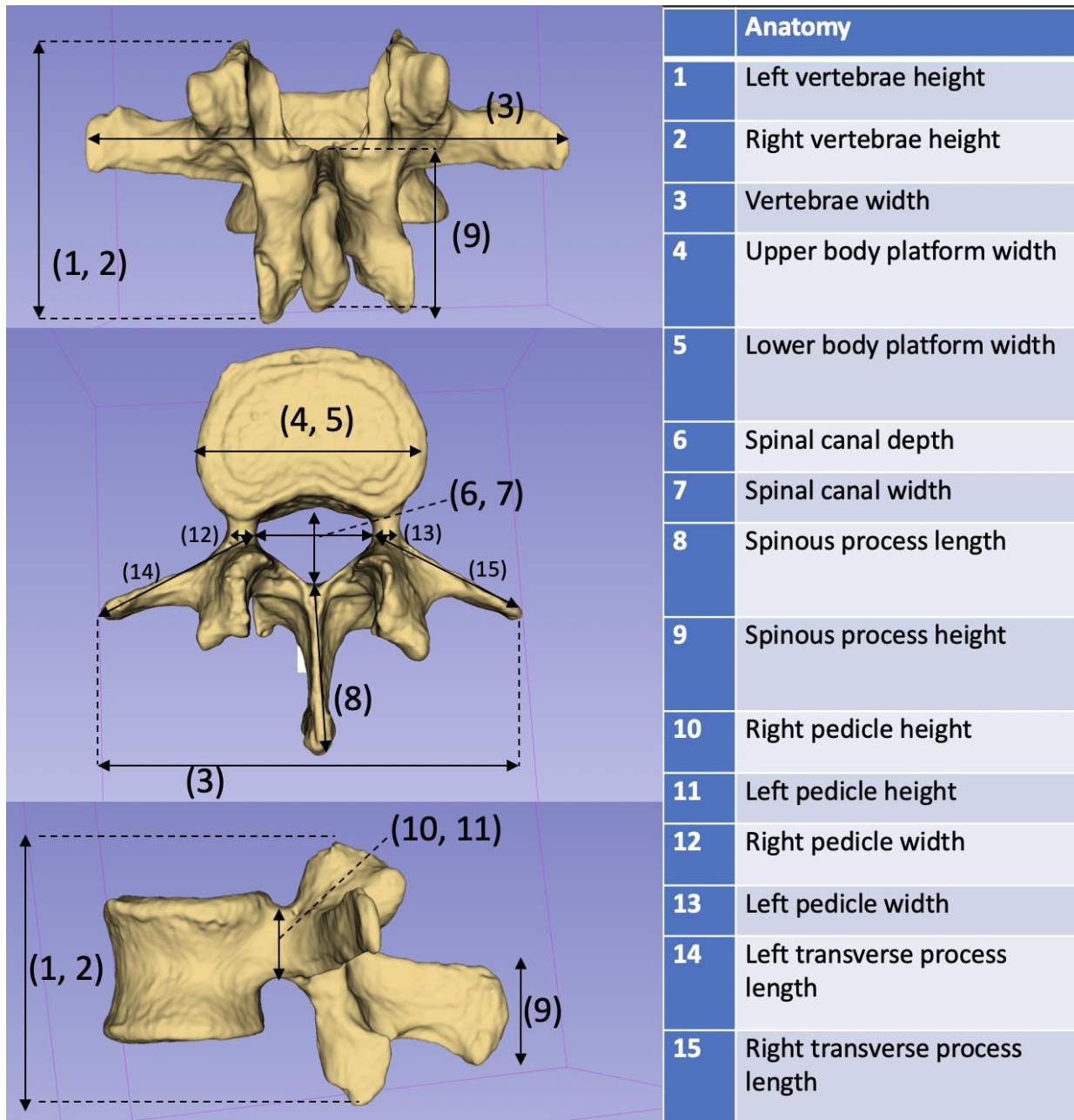


Figure 2

15 vertebral measurement parameters.

Statistical analysis was performed with SPSS software ver. 20.0 (SPSS Inc., Chicago, IL).

The average of all anatomical locations (Left vertebrae height, Right vertebrae height,

Vertebrae width, Upper body platform width, Lower body platform width, Spinal canal depth, Spinal canal width, Spinous process length, Spinous process height, Right pedicle height, Left pedicle height, Right pedicle width, Left pedicle width, Right transverse process length, Left transverse process length) was calculated for each specimen. Using the average measure, the inter-rater reliability was assessed using a two-way random effect, absolute agreement, single-rater ICC to assess the degree that raters provided consistency in their measurements across the different model types for each specimen. Similarly, the ICC for intra-rater reliability was calculated to assess the degree that a single rater provided consistency in repeated measurements, separated by a 2-week interval, across the different model types for each specimen.

To compare measurements of each anatomical region, between the different model types, a one-way ANOVA was used with Tukey's test for post hoc analysis. Additionally, measurements between the different model types were compared using a one-way ANOVA with Tukey's test for post hoc analysis. The  $p < 0.05$  value was used to establish statistical significance.

## Results

30 lumbar vertebrae were harvested and selected to be cleaned. After inspection of the 6 CT scans, 2 L5 vertebrae were excluded due to transitional anatomy. Five vertebrae from 2 different spines were excluded due to damage to the vertebral end plates and transverse

processes during the harvesting and cleaning processes. Therefore 23 vertebrae remained for complete analysis of all four model types, including segmentation metric analysis.

There was excellent inter-rater reliability and intra-rater reliability when comparing measurements across the different model types for each specimen, and with repeated measurements across the different model types for each specimen ([Table 1](#)). There was no statistical difference between manual or virtual measurements when comparing all 4 model types (AB, 3DSM, CTM, 3DPM), except for vertebral width, ( $p = 0.044$ ) ([Figure 3](#)). There was no statistical difference when comparing the average of all 15 measurements between all 4 models types ( $p = 0.247$ ) ([Table 2](#)).

Average measure*	n levels	Rater 1 Mean $\pm$ SD	Rater 2 Mean $\pm$ SD	ICC	95% CI	
<b>Inter-rater reliability</b>						
<b>Bone</b>	5	32.0 $\pm$ 1.4	32.1 $\pm$ 1.2	0.972	0.782	0.997
<b>CT</b>	5	32.6 $\pm$ 1.4	32.5 $\pm$ 1.2	0.988	0.905	0.999
<b>3D Scan</b>	5	32.1 $\pm$ 1.3	32.0 $\pm$ 1.1	0.986	0.892	0.999
<b>3D Print</b>	5	32.8 $\pm$ 1.3	32.8 $\pm$ 1.1	0.977	0.798	0.998

Average measure*	n levels	Measure 1 Mean $\pm$ SD	Measure 2 Mean $\pm$ SD	ICC	95% CI	
<b>Intra-rater reliability</b>						
<b>Bone</b>	5	32.0 $\pm$ 1.4	32.1 $\pm$ 1.4	0.995	0.959	0.999
<b>CT</b>	5	32.6 $\pm$ 1.4	32.6 $\pm$ 1.3	0.997	0.968	1.000
<b>3D Scan</b>	5	32.1 $\pm$ 1.3	32.2 $\pm$ 1.3	0.997	0.976	1.000
<b>3D Print</b>	5	32.8 $\pm$ 1.3	32.9 $\pm$ 1.4	0.997	0.979	1.000

Table 1

Inter-rater and intra-rater reliability regarding Bone, CT, 3D scanned and 3D printed specimens: intraclass correlation coefficient for two raters and two measures by the same rater.



## Multiple Comparisons

Dependent Variable: Average

	(I) Type4	(J) Type4	Mean Difference (I-J)	Std. Error	Sig.	95% Confidence Interval	
						Lower Bound	Upper Bound
Tukey HSD	Bone	CT	-.82990	1.11581	.879	-3.7438	2.0840
		3d Scan	-.42958	1.17489	.983	-3.4978	2.6386
		3d print	.83395	1.11581	.878	-2.0800	3.7479
	CT	Bone	.82990	1.11581	.879	-2.0840	3.7438
		3d Scan	.40031	1.17489	.986	-2.6679	3.4685
		3d print	1.66384	1.11581	.447	-1.2501	4.5778
	3d Scan	Bone	.42958	1.17489	.983	-2.6386	3.4978
		CT	-.40031	1.17489	.986	-3.4685	2.6679
		3d print	1.26353	1.17489	.705	-1.8047	4.3317
	3d print	Bone	-.83395	1.11581	.878	-3.7479	2.0800
		CT	-1.66384	1.11581	.447	-4.5778	1.2501
		3d Scan	-1.26353	1.17489	.705	-4.3317	1.8047
Bonferroni	Bone	CT	-.82990	1.11581	1.000	-3.8316	2.1718
		3d Scan	-.42958	1.17489	1.000	-3.5902	2.7311
		3d print	.83395	1.11581	1.000	-2.1678	3.8357
	CT	Bone	.82990	1.11581	1.000	-2.1718	3.8316
		3d Scan	.40031	1.17489	1.000	-2.7603	3.5610
		3d print	1.66384	1.11581	.834	-1.3379	4.6656
	3d Scan	Bone	.42958	1.17489	1.000	-2.7311	3.5902
		CT	-.40031	1.17489	1.000	-3.5610	2.7603
		3d print	1.26353	1.17489	1.000	-1.8971	4.4242
	3d print	Bone	-.83395	1.11581	1.000	-3.8357	2.1678
		CT	-1.66384	1.11581	.834	-4.6656	1.3379
		3d Scan	-1.26353	1.17489	1.000	-4.4242	1.8971

Table 2

One-way ANOVA and Tukey's for post-hoc analysis, demonstrating no statistical difference when comparing the average of all 15 measurements between all 4 models types ( $p = 0.247$ ).

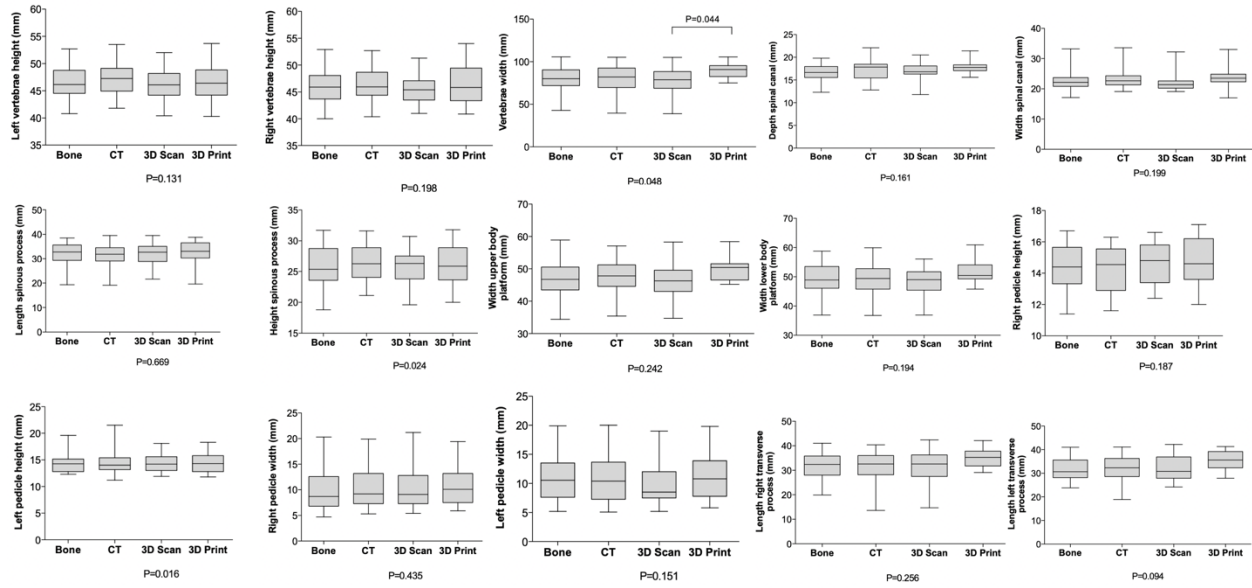


Figure 3

Box-and-whisker plots of the 15 measurements comparing the 4 model types. There was no statistical difference between manual or virtual measurements when comparing all 4 model types (AB, 3DSM, CTM, 3DPM), except for vertebral width when comparing 3DSM and 3DPM ( $p < 0.05$ ).

The mean Hausdorff distance was 0.99 mm (SD 0.55mm) when comparing 3DSM to CTM, signifying approximately 1mm difference between the 2 models ([Figure 4](#)). The mean Dice Coefficient was 0.90 (SD 0.07) when comparing 3DSM to CTM, indicating excellent geometric overlap. The mean volume for 3DSM and CTM were 41.6ml and 45.9ml ( $p < 0.001$ ), respectively, indicating the CTM had a statistically significantly larger volume than the 3DSM.

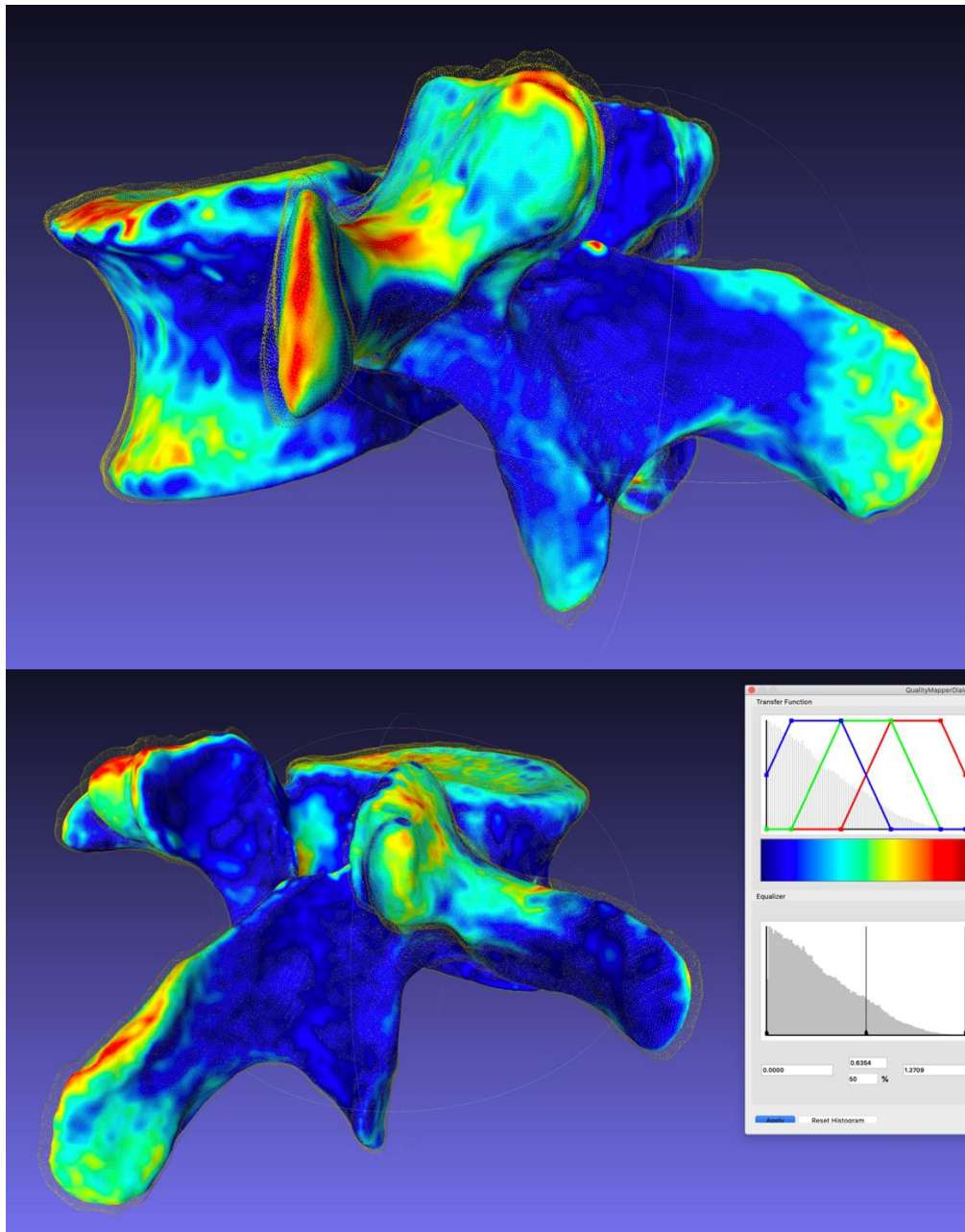


Figure 4

Digital comparison of an L3 vertebra. The outer mesh model was created from the CT scan, which is larger than the solid inner 3D scanned bone. The heat map demonstrates which colours correspond to the changing distance difference. In this example there was a mean Hausdorff distance of 0.64mm (inset).

## Discussion

3D-printing is an ever-expanding field in medicine. Production of 3D-printed medical models and patient-specific instruments are becoming more popular in spine surgery due to multiple benefits, including increased accuracy, affordability, safety of use, and rapid turn-over times <sup>6</sup>. To support the use of 3D-printing, it is necessary to validate the accuracy of medical imaging in the creation of medical models and corresponding patient-specific guides. This study is the first to examine the relationship between human lumbar vertebrae, 3D scans of these bones, CT based models and 3D-printed models. We found no significant differences between manual and virtual measurements of the 4 different types of models, except for vertebral width. However, when studying these models with segmentation metric analysis, we found CTM to be on average 4.3ml larger than their corresponding 3DSM. This was in keeping with an average Hausdorff distance of 0.99mm ([Figure 4](#)). These findings are most significant when applied to the field of 3D-printing, and help to explain the excellent geometric fit of 3D-printed patient specific guides due to the accurate representation of the CTM compared to the bone. If the CTM volume was smaller than the 3DPM/AM then theoretically 3D printed patient-specific guides would not fit on the bones.

Several sources of error can arise when comparing the human skeleton to the various models we have examined in this study. The first can occur if the bone is inadvertently damaged during the removal of soft tissues. By boiling the bones, we found the soft tissues were far easier to

remove, therefore minimizing the chance of inadvertent damage and geometry change. However, some slender and delicate structures, such as the transverse processes and the vertebral body end-plate periphery, were damaged in some cases. This explains the reason for the greater error in AB measurements of vertebral width. These thin and slender anatomical areas can also be easily distorted during the segmentation and smoothing processes.

In theory the process of boiling and drying of bones could cause changes to the geometry but this has also been studied and shown not to be the case. Lander et al. concluded that there were no significant differences between boiling, freezing and degreasing of bone when examining its microstructure, however erosion pits on the surface were visualized using electron microscopy <sup>7</sup>. Galves et al. performed CT scans of porcine lumbar spines before and after soft tissue removal, and found no significant difference between measurements in each group <sup>5</sup>. Therefore, the error that may be produced by boiling and removing soft tissue is not likely to be significant.

The accuracy of a 3D printed model can be cumulatively affected by errors in each step involved in creation of models. These steps include acquisition of imaging, segmentation, and postprocessing of the segmentations. Segmentation is an important step of image-processing, which classifies regions of an image according to the presence of relevant anatomic features <sup>8</sup>. One of the largest sources of inaccuracy in the 3D-printing production line is the segmenting of the imaged tissues <sup>9</sup>. CT segmentation of structures can be affected when the bone-soft tissue interface is indistinct. Smoothing effects are helpful to reduce artefact during the segmentation

process, but often at the expense of model detail and can reduce the size of models. Ogden et al. used different automated threshold-based segmentation techniques to examine the differences between dry bones and 3D printed models. Very small changes in the range of attenuation thresholds changed the difference between bone and 3D printed model from 0.8mm with one threshold, to 1.5mm with another threshold <sup>10</sup>. We used a region-growing, or 'grow-from-seeds' technique, without threshold masking, to create our CTM. This technique relies on a selection of initial seed points, and then adds regions of neighboring pixels to the segmentation. This is a slightly more time-consuming process but results in a more accurate and realistic model. During the segmentation process, we were very careful to compare the final segmentation model to the axial, sagittal and coronal 2D reconstructions, and modify the 'seeds' accordingly. This ensured an excellent match between segmentation and anatomical structure in question. Fortunately, structures such as the transverse processes are rarely used for the application of surgical guides, therefore, the clinical significance of these inaccuracies is minimal.

When comparing the AB to the 3DSM, it is important to quantify how well the virtual model created from the 3D scan reproduces the object being digitized <sup>11</sup>. Several studies have validated the use of the NextEngine laser scanner, with reported average deviations of 0.050mm between virtual models and micro-CT scans of Neanderthal teeth and bones <sup>12</sup>. Perrone et al. found that the NextEngine laser scanner could accurately detect small surface amplitudes as small as 0.1mm, with test-retest measurements differing by no more than 0.137mm <sup>11</sup>. We ensured our scanner was calibrated by scanning a 20mm sphere test object,

which measured 20.12mm on average using a virtual caliper, which is consistent with the published data above. Therefore, the 3DSM can be arbitrarily be used to represent the AB. Appropriately calibrated CT systems have excellent dimensional accuracy, with errors of less than 0.1mm reported <sup>13</sup>. Our established difference between 3DSM and CTM of 0.99mm is expected to be significant, and not due to inaccuracies produced by the 3D or CT scanning process. This difference unlikely to be of diagnostic significance, however it is clinically significant when relating this information to 3D-printing.

Using manual measurements with a caliper is a reliable way of determining whether two structures have a similar size and shape. We showed a high level of agreement and no difference between the manual measurements of the four different model types ([Table 1](#) and [2](#), [Figure 3](#)). However, given the complexity of geometry of the human spine, there are several sources of error that arise during these manual measurements, and very small differences can be overlooked. Manual measurements performed with calipers are operator dependent, rely on precise identification of landmarks, and a small number of measurements may be insufficient for full quantification of complex anatomical structures. Additionally, a small change in the tangent of measurement can result in large changes to the measured value. This can be avoided with the use of 3D models printed with fiducial markers <sup>14</sup>.

When attempting to take measurements of a 3D object on a 2D screen, it is often difficult to place fiducial markers at the widest point of the structure, adding another source of inaccuracy



to the virtual measurements. Despite this difficulty, there was no statistical difference between all four model types.

In order to attempt to detect differences too small to measure with a manual or virtual caliper, digital segmentation comparisons of these complex structures were performed. By digitally aligning and analyzing the 3DSM and CTM it was relatively easy to tell where gross differences exist by visual inspection ([Figure 4](#)). However, to compare models objectively the Dice Coefficient and Hausdorff distance are common techniques used in medical imaging to evaluate segmentation differences, observer agreements and assist in medical and surgical planning (e.g. the detection and monitoring of progressive tumor sizes)<sup>15, 16,17</sup>. A Dice Coefficient of 0.9 in our study indicates excellent spatial overlap when comparing 3DSM and CTM. The average Hausdorff distance in this study was 0.99mm, indicating an average distance difference of approximately 1mm between the CTM and 3DSM.

By calculating the Dice Coefficient and Hausdorff index, very small differences in shape and size can be calculated. On gross inspection, we found that the CTM was consistently larger than the 3DSM in every specimen, in every direction. This was supported by the 3D comparison segmentation metrics. Dice Coefficient calculations demonstrated excellent geometric overlap, with an average score of 0.9. Hausdorff distance calculations demonstrated excellent geometric similarities between the CTM and 3DSM, with an average of 0.99 mm difference between the CTM and 3DSM, and the CTM 4.3 ml larger than the 3DSM on average.

The methodology of comparing cadaveric specimens to 3D printed models has been applied to all major 3D printing technologies, particularly maxillofacial, skull and appendicular bones <sup>14</sup>. However, there is an extremely large gap when applying this knowledge to spinal osteology. Galvez et al. examined the error measurement between porcine lumbar spines, CT images and printed models <sup>5</sup>. Their study revealed an average total error of 0.60mm between the CT model and printed model, and 0.73mm between the printed model and anatomical specimen. The most affected measurements in this study were the width of the spinal canal, length of the right transverse process, height of the spinous process, and right and left pedicle height. These findings are consistent with our study; however, they did not digitize the bones, and therefore could not perform any segmentation metrics.

When producing a 3D printed model, printing inaccuracies can arise. Current studies suggest that the accuracy and reproducibility of professional desktop 3D printer are better than 0.5mm for x-y-axis and z-axis resolution, which is comparable to the spatial resolution of most clinical imaging modalities <sup>14</sup>. The x-y resolution of SLA printers, such as the one used in this study, is determined by the laser beam diameter, which is approximately 0.1-0.2mm. For most SLA machines, the minimal feature size is about 1.5 times the laser beam diameter. Accuracy, on the other hand, measures the degree of agreement between the geometry of the planned and printed object. Wu et al. examined 45 spine CTs and found that 88.6% of the parameters of cervical vertebrae, 90% of thoracic vertebrae and 94% of lumbar vertebrae had an intraclass correlation coefficient (ICC) values of >0.800 between radiographic images and 3D printed spine models <sup>4</sup>. Therefore, excluding print failures, the actual 3D printing process is far less likely to

result in inaccuracies compared to those that occur during the segmentation process, which is highly user dependent. The accuracy of the final 3D printed object can only be as accurate as the segmented model. Visual inspection of our 3DPM confirmed there were no print failures when compared to the corresponding CTM STL file. This accuracy of 3D printing has been reproduced in our study, which show no significant difference between CTM and 3DPM.

## Conclusion

This study clarifies the geometric and volumetric relationship between human lumbar vertebra and CT based vertebral models. The use of segmentation metrics reveals an average of 1mm difference between examined bones (using the 3DSM as a surrogate), and the CT measurements. This is confirmed by a volumetric difference of 4.3ml, between the larger CTM and the smaller AB/3DSM. This study sheds light on the topic of 3D-printing in spinal surgery, and its applications to patient-specific instruments.

## Chapter 2 Reference list

1. Bücking TM, Hill ER, Robertson JL, Maneas E, Plumb AA, Nikitichev DI. From medical imaging data to 3D printed anatomical models. Chen H-CI, ed. *PLoS ONE*. 2017;12(5):e0178540. doi:10.1371/journal.pone.0178540
2. Brouwers L, Teutelink A, van Tilborg FAJB, de Jongh MAC, Lansink KWW, Bemelman M. Validation study of 3D-printed anatomical models using 2 PLA printers for preoperative

planning in trauma surgery, a human cadaver study. *Eur J Trauma Emerg Surg*.

2019;45(6):1013-1020. doi:10.1007/s00068-018-0970-3

3. Reddy MV, Eachempati K, Gurava Reddy AV, Mugalur A. Error Analysis: How Precise is Fused Deposition Modeling in Fabrication of Bone Models in Comparison to the Parent Bones?

*Indian J Orthop*. 2018;52(2):196-201. doi:10.4103/ortho.IJOrtho\_312\_16

4. Wu A-M, Shao Z-X, Wang J-S, et al. The Accuracy of a Method for Printing Three-Dimensional Spinal Models. Zhang H, ed. *PLoS ONE*. 2015;10(4):e0124291.

doi:10.1371/journal.pone.0124291

5. Galvez M, Montoya CE, Fuentes J, et al. Error Measurement Between Anatomical Porcine Spine, CT Images, and 3D Printing. *Academic Radiology*. July 2019:S1076633219303228.

doi:10.1016/j.acra.2019.06.016

6. Kim SB, Won Y, Yoo HJ, et al. Unilateral Spinous Process Noncovering Hook Type Patient-specific Drill Template for Thoracic Pedicle Screw Fixation: A Pilot Clinical Trial and Template

Classification. *Spine (Phila Pa 1976)*. 2017;42(18):E1050-E1057.

doi:10.1097/BRS.0000000000002067

7. Lander SL, Brits D, Hosie M. The effects of freezing, boiling and degreasing on the

microstructure of bone. *Homo*. 2014;65(2):131-142. doi:10.1016/j.jchb.2013.09.006

8. Zou KH, Warfield SK, Bharatha A, et al. Statistical validation of image segmentation quality based on a spatial overlap index1. *Academic Radiology*. 2004;11(2):178-189.

doi:10.1016/S1076-6332(03)00671-8

9. Huotilainen E, Jaanimets R, Valášek J, et al. Inaccuracies in additive manufactured medical skull models caused by the DICOM to STL conversion process. *J Craniomaxillofac Surg*. 2014;42(5):e259-265. doi:10.1016/j.jcms.2013.10.001
10. Ogden KM, Aslan C, Ordway N, Diallo D, Tillapaugh-Fay G, Soman P. Factors Affecting Dimensional Accuracy of 3-D Printed Anatomical Structures Derived from CT Data. *J Digit Imaging*. 2015;28(6):654-663. doi:10.1007/s10278-015-9803-7
11. Perrone RV, Williams JL. Dimensional accuracy and repeatability of the NextEngine laser scanner for use in osteology and forensic anthropology. *Journal of Archaeological Science: Reports*. 2019;25:308-319. doi:10.1016/j.jasrep.2019.04.012
12. Slizewski A, Astrid, Friess M, Martin, Semal P, Patrick. Surface scanning of anthropological specimens: nominal-actual comparison with low cost laser scanner and high end fringe light projection surface scanning systems. *Quartär*. 2010;57:179-187.
13. Engelke K, Libanati C, Liu Y, et al. Quantitative computed tomography (QCT) of the forearm using general purpose spiral whole-body CT scanners: Accuracy, precision and comparison with dual-energy X-ray absorptiometry (DXA). *Bone*. 2009;45(1):110-118. doi:10.1016/j.bone.2009.03.669
14. George E, Liacouras P, Rybicki FJ, Mitsouras D. Measuring and Establishing the Accuracy and Reproducibility of 3D Printed Medical Models. *RadioGraphics*. 2017;37(5):1424-1450. doi:10.1148/rg.2017160165
15. Dice LR. Measures of the Amount of Ecologic Association Between Species. *Ecology*. 1945;26(3):297-302. doi:10.2307/1932409

16. Taha AA, Hanbury A. Metrics for evaluating 3D medical image segmentation: analysis, selection, and tool. *BMC Med Imaging*. 2015;15(1):29. doi:10.1186/s12880-015-0068-x
17. Bagci U, Udupa JK, Mendhiratta N, et al. Joint segmentation of anatomical and functional images: Applications in quantification of lesions from PET, PET-CT, MRI-PET, and MRI-PET-CT images. *Medical Image Analysis*. 2013;17(8):929-945. doi:10.1016/j.media.2013.05.004
18. Zijdenbos AP, Dawant BM, Margolin RA, Palmer AC. Morphometric analysis of white matter lesions in MR images: method and validation. *IEEE Trans Med Imaging*. 1994;13(4):716-724. doi:10.1109/42.363096

## Chapter 3: The Development of novel 2-in-1 patient specific, 3D-printed laminectomy guides with integrated pedicle screw drill guides

Key words:

Human spine.

Lumbar spine.

3D-printing.

Image Processing, Computer-Assisted.

CT.

Pedicle screw.

Laminectomy.

### Introduction

Laminectomy is the mainstay of treatment for spinal conditions that require decompression of the neural elements, such as spinal stenosis, spondylolisthesis, intervertebral disc herniation and fracture <sup>1 2</sup>. Over the past decade, there has been a rise in the need for spine decompression for lumbar conditions <sup>3</sup>. Despite being a very common procedure, spinal decompression using traditional laminectomy has several risks, including dural tear, damage to neural elements and spinal instability due to iatrogenic spondylolisthesis <sup>4</sup>.

Pedicle screw fixation is the workhorse of posterior fixation and fusion techniques for the thoracic and lumbar spines <sup>5</sup>. A variety of screw insertion techniques currently exist, each with

specific advantages and disadvantages. Traditional methods of pedicle screw implantation include free-hand techniques or use of 2-dimensional (2D) intraoperative x-ray (fluoroscopy). More advanced techniques for pedicle screw implantation include intraoperative navigation and robotic-assisted techniques.

Complications of screw mal-positioning include nerve root injury, dural tear, vascular injury and infection. Insertion accuracy in the lumbar spine is higher than in the thoracic spine due to larger pedicles and more distinct anatomy<sup>6</sup>. Thoracic pedicle screw perforation rate using free-hand techniques ranges from 25% to 43%. Anatomical difficulty and technical inexperience are reasons for complications related to free-hand pedicle screw misplacement<sup>7 8 9</sup>. Lumbar pedicle screw perforation rates are reported to be approximately 14%, with 3.3% being perforated 4mm or more, and neurological complications occurring in 25.8% of these perforations. Neurological complications occur in 89.2% of cases in which a pedicle screw has perforated medially or inferiorly<sup>10</sup>.

Traditional intraoperative fluoroscopy and navigation platforms exposes the surgical team and patient to potentially large doses of radiation<sup>11</sup>. However the rate of pedicle screw perforation improves to 5.1% - 13.4% for fluoroscopy assisted surgery<sup>12</sup>. The use of navigation results in overall reported rate of screw malposition of 8.5% -11%<sup>13</sup>.

Traditional and more advanced screw insertion techniques, such as navigation, still play an important role in spine surgery; however, their deficiencies have led to increased interest in



other techniques, including the use of PSG. The main reported advantages of PSGs include: low costs, improved turnover times, minimal risk for patient and surgical team, reduced radiation exposure for surgical teams, and improvements in precision and sizing of surgical instrumentation due to guide individualization which allow for inter-segmentary motion <sup>14</sup>. Several different designs of patient-specific guides have been described, however there are no guidelines regarding minimum standardisation in their design and protocols <sup>9</sup>. Currently, the use of patient specific guides in spine surgery has been largely restricted to drill guides for pedicle screws.

To our knowledge, the use of PSG has not been applied to laminectomy. Additionally, modular 2-in-1 guides, which include laminectomy guides and integrated, removable pedicle screw drill guides, have not been designed or tested. The aim of study is to design and test novel patient-specific laminectomy guides. Laminectomy guides will be location and depth specific to determine if neural decompression can be performed efficiently and safely in a pre-planned location. Pedicle screws will be inserted with assistance of an integrated drill guide that can fit into the laminectomy guide when attached to the spinous process ([Figure 1](#)).

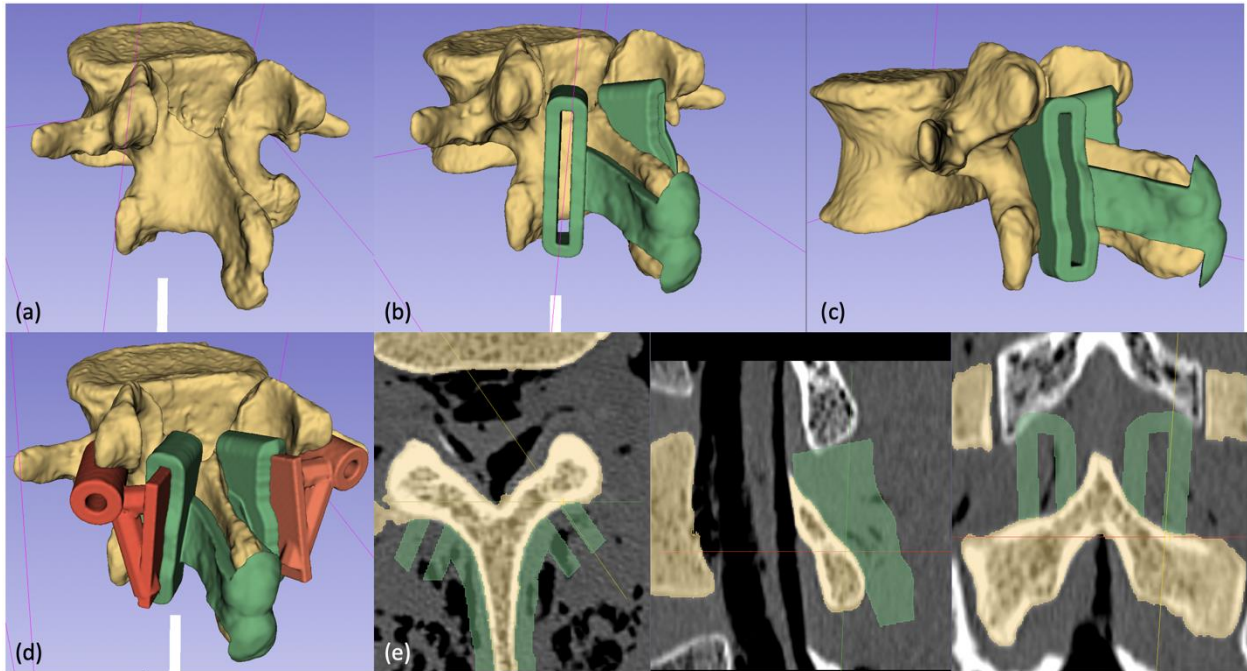


Figure 1

(a) A 3D model of the vertebra was created using 3D Slicer. (b), (c) Longitudinal laminectomy guides were placed in the appropriate position and connected to a template placed on the spinous process. (d) Drill guides were created to assist in pedicle screw insertion and joined to removable slots which fit into the laminectomy guides, to create a 2-in-1 guide. (e) Axial, sagittal and coronal reconstructions demonstrating how the laminectomy guides were designed to match the deep surface of lamina, to create a 14mm depth-stop design.

## Methods

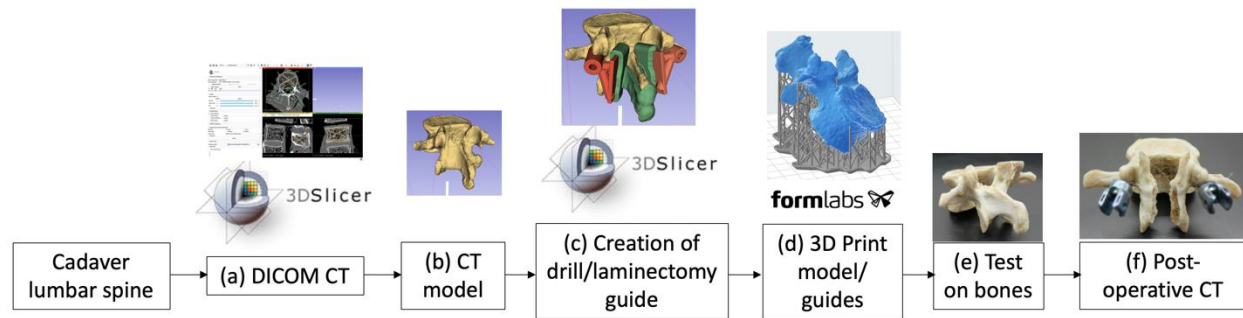


Figure 2

Overview of the image processing, 3D printing and testing steps. 3D Slicer software was obtained from slicer.org.

### Medical imaging:

After institutional ethics approval, three of the complete human cadaver spines and the DICOM files used in Chapter 2 were utilized ([Figure 2](#)).

### Soft tissue removal:

The cleaned bones described in Chapter 2 were utilised.

### Images processing, segmentation and creation of patient-specific guides ([Figure 2a-c](#)):

Vertebral models were created using the same methods as in Chapter 2.

Patient-specific templates were constructed using 3D Slicer ([Figure 2c](#)). The first step involved making a 3mm hollow shell from the vertebral model. This shell was trimmed to create the template which rested on the spinous process and lamina ([Figure 1a](#)). Longitudinal lamina osteotomy guides were placed in the appropriate position to simulate preservation of the facet joints and pars interarticularis ([Figure 1b-d](#)), however the position of these guides could easily be tailored to surgeon preference. The guides were 2.5mm wide, to accommodate a 2.5mm match head burr (for example T12MH25 Medtronic Inc. <sup>TM</sup> MIDAS REX, Memphis, TN, USA) and spanned the length of the lamina. The dorsal contour of the laminar osteotomy guides was created to match the deep surface of the lamina, set at a depth of 14mm ([Figure 1e](#)). This theoretically ensures that the burr tip will travel along the dorsal aspect of the ligamentum flavum and dura, if the burr tip is offset 14mm from the handle piece.

The pedicle width was measured in order to template screw width. Appropriately sized cylinders (4.5mm – 7.5mm diameter) were created and placed in the ideal trajectory of the pedicle screws. The cylinder diameter was made approximately 80% of the narrowest cross-sectional diameter of the pedicle <sup>15</sup>. Cylinders, rather than screws with threads, were used to plan screw trajectory to allow accurate and direct visualization of potential breaches, in different planes, on the 2D and 3D reconstructions. The ideal trajectory was judged by the cylinder being in the centre of the pedicle in all 3 planes, parallel to the superior endplate, and avoiding breach of the facet joint. All screws were planned completely inside the pedicle if possible. If the pedicle diameter was smaller than the smallest available screw (4.5mm), planned in-out-in approaches were created, with the cylinder placed adjacent to the medial

pedicle wall. Safe screw length was measured by using the distance between the entry point and anterior vertebral body surface, in line with the cylinder. 4mm diameter drill guides were created around the planned trajectory of the pedicle screws. The drill guides were made 10mm long to allow the burr, set to a 14mm depth for the laminectomy, to decorticate the entry point and to perform the laminectomy without changing burr handle settings. The drill guides were then attached to slots that could be inserted and removed from the laminectomy guides ([Figure 1e](#), [Figure 3a-b](#)). This was done in order to facilitate smooth workflow and efficiency of printed parts, making it necessary to print only one template set (3 parts) per spinal level, which included the lamina template and 2 drill guides.

### 3D Printing of Patient-specific guides:

The patient-specific templates and hollow vertebral bio-model files were exported as STL files and imported into Formlabs Preform software (Version 3.0.2), to be printed using Formlabs Form 2 (Formlabs Inc. Somerville, MA) desktop 3D printer. The templates were oriented on the build platform to avoid placing supports on parts of the templates that would be in contact with the bone ([Figure 2d](#)). The z-axis layer thickness was set to 0.1mm. GreyPro resin was used as it has a long shelf life, and closely resembled the material properties of Surgical Guide Resin, which has a 3-month shelf life. The Surgical Guide resin is fully biocompatible, and can be steam sterilized using an autoclave, allowing it to be used safely in the clinical setting.

### Pre-operative assessment ([Table 1](#)):

The following segmentation parameters were recorded: vertebral model segmentation duration, per level; and template planning duration, per level.

The following 3D-printing parameters were recorded: vertebral model print time and volume of resin required per level; and template print time and volume of resin required per level.

#### Testing of patient-specific guides:

Prior to testing, the template was placed onto the 3D printed vertebral bio-model to ensure ease of application, and a secure fit with close apposition of the adjacent surfaces of the template and the bio-model ([Figure 3a](#)). In general, a snap fit occurred over the spinous process, and there was only one way the guide could fit, which made the assessment of fit quite easy. A laminectomy guide test simulation was performed on the bio-model to ensure the burr tip did not travel deep to the inner table margin of the lamina. None of the templates required modifications at this point.

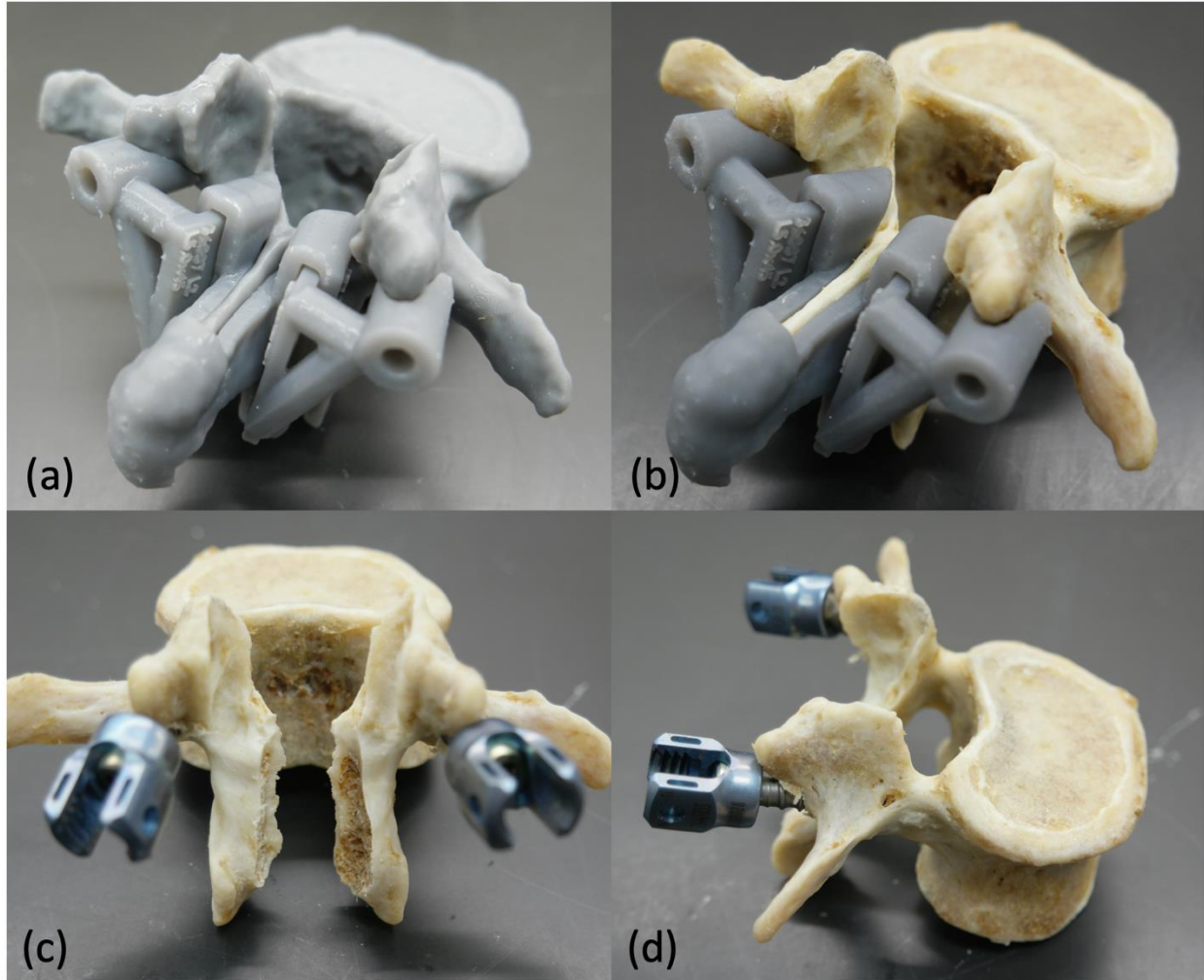


Figure 3

(a) The 2-in-1 template was placed onto 3D printed L2 vertebra preoperatively to ensure the stability of the template and ease of fit. (b) The template placed on the corresponding bone for testing. (c) and (d) Posterior and right lateral views of the vertebral after laminectomy and pedicle screw placement.

An assistant held the vertebral body during testing, and the surgical procedure was performed by a spine surgeon (PR) who was blinded to the surgical planning ([Figure 2e](#)). The lamina template with laminectomy guide was placed on the bone. A good fit and position were confirmed visually ([Figure 3b](#)). Gentle downward finger pressure was placed on the template and one 2mm k-wire with an olive was placed into a predrilled hole adjacent to the dorsal aspect of the spinous process. This prevented the guide from lifting off during the drilling and burring steps. The drill guides with slots were fit into the lamina osteotomy guides ([Figure 3b](#)). The entry points for the screws were decorticated through the drill guides, using a T12MH25 Medtronic MIDAS REX 2.5mm match head burr. Particular attention was placed on burring the caudal and lateral aspect of the mammillary process to ensure the drill did not slide laterally off this projection of bone in the next step. A 4mm drill with short flutes was placed through the drill guides and the screw path was drilled to a length of 40mm. The drill guides were removed from the laminectomy slots. The path was probed for deficits with a firm pedicle feeler, and then tapped line-to-line with the planned screw. The pre-planned CD Horizon Legacy (Medtronic Inc. <sup>TM</sup>; Sofamor Danek, Memphis, TN, USA) screws were inserted ([Figure 3c-d](#)). The laminectomies were performed bilaterally through the laminectomy guides using the burr set to a pre-planned 14mm depth. The spinous process and lamina were removed with the laminectomy guide on-bloc ([Figure 3 c-d](#)).

Intraoperative assessment ([Table 1](#)):



The under-surface of the lamina was filmed during the laminectomy, using a high-definition digital camera, in order to determine the burr tip position compared to the inner table of the lamina.

Surgical times for each vertebral level were recorded; starting at the time the template was secured to the bone to when the laminectomy was complete.

Postoperative assessment ([Table 1](#)):

The bones were directly visually inspected to detect any cortical breach around the pedicle or anterior vertebral body. Laminectomies were judged as successful if the burr tip did not pass deep to the inner table margin on the digital recording.

Postoperative CT scans were performed using a metal-reduction protocol ([Figure 2f](#)). The accuracy of screw positioning was confirmed using the classification according to Mirza et al.<sup>6</sup>: grade 0 – no cortical breach; grade 1 – cortical perforation with protrusion of the screw <2mm; grade 2 – cortical perforation <4mm; grade 3 – cortical perforation >4mm.

The individual vertebra and screws were segmented postoperatively using the semi-automated 'grow from seeds' extension in the Segment Editor of 3D Slicer. The planned and actual vertebral models were imported as STL files into Meshlab (v. 1.3.2, Consiglio Nazionale delle Ricerche – CNR, Rome, Italy). The two models were aligned using an iterative closest point

algorithm (point based gluing tool). At least 3 fiducial points were used to ensure the models were aligned appropriately. The aligned models were imported back into 3D Slicer, where axial and sagittal angular differences were measured using an on-screen protractor. The difference between the planned and actual screw angle in the axial plane was defined as the axial screw error. Correspondingly, the difference between the planned and actual screw angle in the sagittal plane was defined as the sagittal screw error <sup>16</sup>.

The deviation distance between the planned and actual screw was measured in the coronal plane at the midpoint of the pedicle <sup>17</sup>. The planned and actual laminectomy widths were recorded, at the most cranial and caudal aspects of the laminae. Correspondingly, the planned and actual remaining width of the mid-pars interarticularis were measured.

#### Statistical analysis:

Means and standard deviations for continuous variables are presented. Data was analysed by using SPSS software ver. 20.0 (SPSS Inc., Chicago, IL). A paired student's T-test was used to compare the planned and actual laminectomy distances, as well as the remaining width of the mid-pars interarticularis.  $P \leq 0.05$  were considered statistically significant.

## Results

Variable	Result	
Cortical breaches	0	
Mean axial screw error	2.5 deg	SD 1.7
Mean sagittal screw error	0.6 deg	SD 1.2
Mean distance deviation at pedicle midpoint	1.1mm	SD 0.75
Deep Laminectomy passes	0	
Average surgical time	4min 46 sec	SD 1min 38sec
Average vertebral segmentation time	33 min	SD 6 min
Average template design time	77 min	SD 19 min
Average vertebral print time	4 h 46 min	SD 55 min
Average template print time	3 h 39 min	SD 32 min
Average vertebral print volume	36.5 ml	SD 4.6 ml
Average template print volume	17.6 ml	SD 2.5 ml
	<b>Planned</b>	<b>Actual</b>
Cranial laminectomy width	13.3 mm	13.7mm (p = 0.22)
Caudal laminectomy width	16.9 mm	17.4 mm (p = 0.28)
Width of pars-interarticularis	10.4 mm	9.7 mm (p < 0.05)

Table 1

Summary of results.

### Screw analysis:

In total, 30 screws were inserted in 15 lumbar vertebrae by using the integrated 2-in-1 patient-specific drill guides. There were no cortical breaches on direct examination, or on postoperative CT (grade 0), in any case or in any direction ([Table 1](#)). The mean axial screw error was 2.5 degrees (SD 1.7). The mean sagittal screw error was 0.6 degrees (SD 1.2). The mean distance deviation between planned and actual screw position at the midpoint of the pedicle in the coronal plane was 1.1mm (SD 0.75).

### Laminectomy analysis ([Table 1](#)):

Digital video analysis revealed the burr tip did not pass deep to the inner table margin of the lamina in any of the 30 laminectomy cuts. In one vertebra, the burr passage was too shallow bilaterally, and the laminectomy was incomplete due to insufficient bone removal.

There was no significant difference between mean planned and actual width of cranial aspect of the laminectomy, measuring 13.3mm and 13.7mm, respectively ( $p = 0.22$ ). There was no significant difference between the mean planned and actual width of caudal aspect of the laminectomy, measuring 16.9mm and 17.4mm, respectively ( $p = 0.28$ ). There was a significant difference between mean planned and actual remaining width of the mid-pars interarticularis, measuring 10.4mm and 9.7mm, respectively ( $p < 0.05$ ).

### Surgical times and print parameters (Table 1):

Average surgical time was 4 minutes and 46 seconds (SD 1m 38s), per level, including positioning of guides, bilateral screw insertion and laminectomy on 15 vertebrae.

The average segmentation time for the vertebral model and corresponding template set was 33 mins (SD 6.5), and 77 mins (SD 19) respectively, on 15 vertebrae.

The average print time for the vertebral model and corresponding template set was 4 hours 46 mins (SD 55 mins) and 3 hours 39 mins (SD 32), respectively.

The average print volume for the vertebral model and corresponding template set was 36.5 ml (SD 4.6) and 17.6ml (SD 2.5).

### Discussion

Pedicle screw insertion and laminectomy are two of the most commonest steps performed in spinal surgery<sup>1-5,7,8</sup>. Complications of these procedures include nerve root or spinal cord injury, dural tear, vascular injury and infection. Recent advances in the field of 3D-printing have sought to simplify the complexity of these challenging aspects of spinal surgery<sup>13,15-21</sup>. In this study, 2-in-1 patient-specific laminectomy guides, with integrated pedicle screw drill guides, were used to safely and efficiently perform these complex and time-consuming steps. The pedicle screws

and laminectomies were performed accurately, with safety of laminectomy confirmed by ensuring the burr tip did not travel deep to the inner table margin of the lamina.

Traditional screw insertion techniques using freehand placement results in perforation rates of 25% to 43% <sup>7,8</sup>. Use of intraoperative fluoroscopy improves perforation rates to 5.1% - 13.4%, but this increases the radiation exposure for the patient and surgical team <sup>11,12</sup>. Recent advances in intra-operative navigation systems have allowed for intraoperative 3D image acquisition which increases accuracy of instrumentation placement. The overall reported rate of screw malposition is 8.5% -11% using navigation techniques <sup>13</sup>. Several weaknesses of these systems include: a significant learning curve; exposure to radiation; optical array devices that can be displaced or obscured by surgical team members or instruments; and high cost. High rates of screw malposition are due to mismatch of navigation and intraoperative position due to inter-segmentary vertebral movement during surgery or optical array shift. Intraoperative navigation requires registration of bone structures which takes varying amounts of time and requires additional personnel during surgery. These additional factors lead to increase surgical time, and therefore, a higher theoretical risk of intraoperative infection <sup>23</sup>.

Several clinical studies have reported excellent screw accuracy when using patient-specific templates in the lumbar spine. Overall screw accuracy rates were 84% - 100%, which is better than free-hand techniques, and equivalent to fluoroscopic- and navigation-assisted techniques ([Chapter 1](#)) <sup>18-20,22,24</sup>. Our study has confirmed the accuracy of screw insertion using 2-in-1 patient-specific drill guides, with no cortical breaches and excellent correspondence between

planned and actual screw position ([Table 1](#)). Another advantage of using 3D imaging to plan surgery is the screw width and length can be optimised, therefore maximising biomechanical properties of each screw <sup>24</sup>. We were concerned that the modularity of our guides would create a source of error, however this did not occur. We found that the high amount of surface contact with the bone around the lamina, as well as the contact of the drill guides on the mammillary processes, ensured stability when drilling and performing the laminectomies.

To our knowledge, the use of custom patient-specific guides to perform lumbar laminectomies is novel and has not been described in the current published literature. In order to assess the safety of these novel guides, we had to formulate a novel approach to assess the burr depth. This was achieved by cleaning the bones and digitally recording the under-surface of the laminectomy. We judged a successful laminectomy as one where the burr tip did not travel deep to the inner laminar table margin. A thin amount of bone was often left at the inner table margin, which was also judged as a success, as the spinous process was easily removed with a gentle torsion force. We found our planned laminectomy position to correspond to the actual position in all cases. The mean of 0.7mm over-resection of bone from the pars, is not clinically significant, and is likely due to the medial-lateral angular tolerance allowed in the guide. A mean of 9.7mm of mid-pars interarticularis remained, which reduces the risk of iatrogenic pars fracture and spondylolisthesis <sup>25</sup>.

Zhang et al. used PSGs to assist in open-door cervical laminoplasty. They designed their 'laminar holders' to accommodate a high-speed drill with a depth limitation device, similar to our

laminectomy guides, so that the drill penetrated the dorsal and ventral cortices of the open side, and only the dorsal cortex on the hinge side. They found that all troughs were at the proper hinge position, with no hinge fracture in the template group. Cervical spine laminae are considerably smaller and have less complex geometry than the lumbar lamina, so the holders in this study were flat in shape, unlike our laminectomy guides.

#### Time utilisation:

Use of PSG to assist in orthopaedic surgery is a time-consuming process in the planning stage. The planning requires specific knowledge of segmentation and 3D-printing software, which is usually done by an engineer. Our models and templates were made by a spine surgeon (AK), which reduced the possibility of error caused by communication breakdown between surgeons and engineers. It took approximately 2 hours to prepare each vertebral model and template set, with an additional 4-6 hours for printing. We found that one Form 2 build platform could accommodate 3-4 vertebral models, or 3-4 template sets, which facilitates efficiency. The entire design and printing process can be completed within a 24-hour window, including post-processing and sterilisation of guides for procedures that required 3-4 sets of guides or less. Our average surgical time was 5 minutes, for accurate insertion of screws and safe laminectomy. We hope that the preoperative planning and preparation time will translate into shorter operative times, with optimal screw choice and position, which will reduce risk of serious complications due to prolonged surgery and implant malposition <sup>26</sup>.



### Cost of production:

Surgical guide resin retails for US \$149 per litre. Therefore, the material cost of one vertebral model is approximately US \$5.50, and one template set costs approximately US \$2.60. We used 3D Slicer, which is an open source platform for research purposes, and is currently not approved by the FDA for clinical use. The cost of software approved for clinical use (such as MIMICS; Materialise, Leuven, Belgium) needs to be considered.

The initial costs of a 3D printer, costs of sterilization, packaging and ongoing costs of an engineer also should be considered, however compared to costs of navigation platforms, 3D-printing is still markedly more cost effective in the long term (see [Chapter 1](#))<sup>27</sup>.

### Limitations:

Several disadvantages exist when using PSGs, with most stemming from inaccuracies that arise during the segmentation of models<sup>28</sup>. Templates require complex designs which require them to guide surgical instruments, and sometimes power tools. They need to be easily positioned and keep their position during use<sup>29</sup>. We found the use of supplemental fixation, via a k-wire with olive, ensured excellent stability of the template throughout the steps of the surgery. Another important feature of templates is to allow the operator to check their position during use, by windows in the guide or by using transparent material. Our laminectomy guides had a

large amount of surface contact to ensure proper fit, and the Surgical Guide resin is transparent, which will ensure ease of use in the clinical setting.

The thorough cleaning of the bones in this study ensured accurate video recording of the laminectomy and ensured ease of fit of the templates. However, this amount of cleaning around the spinous process is time consuming, and the dense supraspinous ligament and fascia are often difficult to remove from the bone. Insufficient removal of soft tissues in these regions can lead to incorrect placement of the guide on the bone in the clinical setting. This in turn, can lead to guide movement from unstable fixation. It is possible to design guides which fit bilaterally or unilaterally, without coverage of the spinous process, which preserves the posterior ligament complex<sup>9</sup>. Bilateral fitting templates are considered to have better stability than unilateral designs but require more soft-tissue removal. We believe the one incomplete laminectomy in this study was due to the guide sitting off the bone by a small fraction. This in turn will lead to under-resection of bone at the deep surface of lamina. Further research is necessary to test our guides in the clinical setting.

The novel use of digital video recording to assess laminectomy safety has not been validated and does not guarantee that the burr tip will not cause damage to the dura or neural elements clinically. We believe this assessment is currently the best possible way to assess this new technique. The use of a side cutting burr with a blunt tip, such as the match head burr, minimises dura or neural injury even if contact occurs. Nevertheless, it is extremely difficult to

recreate a realistic dural tube in the cadaveric laboratory setting<sup>30</sup>, and may require animal tests to determine safety before use on humans.

The use of laminectomy guides, similar to those used in this study, require a burr that has an adjustable length, which is not available in all centres. Ultrasonic bone cutting instruments, such as the Bone Scalpel (Misonix, NY), could theoretically be used to perform the laminectomy with modifications to the width and depth of the laminectomy guides, however these instruments are also not widely available and are additional sources of cost.

Formlabs GreyPro resin was used for all of the templates in this study, because of its similar biomechanical properties to the sterilisable Surgical Guide and Dental SG resins, however it has a longer shelf-life and is more practical for laboratory tests. The Surgical Guide and Dental SG resins require more regular resin tank changes due to damage and wear. Therefore, before clinical application of these guides, further testing will be required using a resin which is biocompatible and safe, such as the Surgical Guide resin.

3D Slicer is an open-source software which can be used for research studies. It has several powerful segmentation tools and is capable of creating models and guides via the 'Segment Editor' and 'Create Models' extensions. It is currently not FDA approved to be used in the clinical setting, therefore, to reproduce this study clinically, a similar FDA approved segmentation tool, such as MIMICS (Materialise, Leuven Belgium), would need to be utilised.

## Conclusion

This study had explored the development of novel 2-in-1 patient specific, 3D-printed laminectomy guides with integrated pedicle screw drill guides, which are accurate and safe in the laboratory setting. These instruments have the potential to simplify complex surgical steps, and improve accuracy, time and cost.

## Chapter 3 reference list

1. Phan K, Mobbs RJ. Minimally Invasive Versus Open Laminectomy for Lumbar Stenosis: A Systematic Review and Meta-Analysis. *SPINE*. 2016;41(2):E91-E100. doi:10.1097/BRS.0000000000001161
2. Zaina F, Tomkins-Lane C, Carragee E, Negrini S. Surgical versus non-surgical treatment for lumbar spinal stenosis. Cochrane Back and Neck Group, ed. *Cochrane Database of Systematic Reviews*. Published online January 29, 2016. doi:10.1002/14651858.CD010264.pub2
3. Machado GC, Maher CG, Ferreira PH, et al. Trends, Complications, and Costs for Hospital Admission and Surgery for Lumbar Spinal Stenosis: *SPINE*. 2017;42(22):1737-1743. doi:10.1097/BRS.0000000000002207
4. Overdevest GM, Jacobs W, Vleggeert-Lankamp C, Thomé C, Gunzburg R, Peul W. Effectiveness of posterior decompression techniques compared with conventional laminectomy for lumbar stenosis. Cochrane Back and Neck Group, ed. *Cochrane Database of Systematic Reviews*. Published online March 11, 2015. doi:10.1002/14651858.CD010036.pub2
5. Belmont PJ, Klemme WR, Robinson M, Polly DW. Accuracy of thoracic pedicle screws in patients with and without coronal plane spinal deformities. *Spine*. 2002;27(14):1558-1566. doi:10.1097/00007632-200207150-00015
6. Mirza SK, Wiggins GC, Kuntz C, et al. Accuracy of thoracic vertebral body screw placement using standard fluoroscopy, fluoroscopic image guidance, and computed tomographic image guidance: a cadaver study. *Spine*. 2003;28(4):402-413. doi:10.1097/01.BRS.0000048461.51308.CD
7. Castro WH, Halm H, Jerosch J, Malms J, Steinbeck J, Blasius S. Accuracy of pedicle screw placement in lumbar vertebrae. *Spine*. 1996;21(11):1320-1324. doi:10.1097/00007632-199606010-00008

8. Vaccaro AR, Garfin SR. Internal fixation (pedicle screw fixation) for fusions of the lumbar spine. *Spine*. 1995;20(24 Suppl):157S-165S.
9. Kim SB, Won Y, Yoo HJ, et al. Unilateral Spinous Process Noncovering Hook Type Patient-specific Drill Template for Thoracic Pedicle Screw Fixation: A Pilot Clinical Trial and Template Classification. *Spine (Phila Pa 1976)*. 2017;42(18):E1050-E1057. doi:10.1097/BRS.0000000000002067
10. Saarenpää I, Laine T, Hirvonen J, et al. Accuracy of 837 pedicle screw positions in degenerative lumbar spine with conventional open surgery evaluated by computed tomography. *Acta Neurochir (Wien)*. 2017;159(10):2011-2017. doi:10.1007/s00701-017-3289-7
11. Pitteloud N, Gamulin A, Barea C, Damet J, Racloz G, Sans-Merce M. Radiation exposure using the O-arm® surgical imaging system. *Eur Spine J*. 2017;26(3):651-657. doi:10.1007/s00586-016-4773-0
12. Oh HS, Kim J-S, Lee S-H, Liu WC, Hong S-W. Comparison between the accuracy of percutaneous and open pedicle screw fixations in lumbosacral fusion. *Spine J*. 2013;13(12):1751-1757. doi:10.1016/j.spinee.2013.03.042
13. Gelalis ID, Paschos NK, Pakos EE, et al. Accuracy of pedicle screw placement: a systematic review of prospective in vivo studies comparing free hand, fluoroscopy guidance and navigation techniques. *Eur Spine J*. 2012;21(2):247-255. doi:10.1007/s00586-011-2011-3
14. Cecchinato R, Berjano P, Zerbi A, Damilano M, Redaelli A, Lamartina C. Pedicle screw insertion with patient-specific 3D-printed guides based on low-dose CT scan is more accurate than free-hand technique in spine deformity patients: a prospective, randomized clinical trial. *Eur Spine J*. 2019;28(7):1712-1723. doi:10.1007/s00586-019-05978-3
15. Maeda T, Higashino K, Manabe H, et al. Pullout Strength of Pedicle Screws Following Redirection After Lateral or Medial Wall Breach: *SPINE*. 2018;43(17):E983-E989. doi:10.1097/BRS.0000000000002611
16. Mathew JE, Mok K, Goulet B. Pedicle violation and Navigational errors in pedicle screw insertion using the intraoperative O-arm: A preliminary report. *The International Journal of Spine Surgery*. 2013;7(1):e88-e94. doi:10.1016/j.ijssp.2013.06.002
17. Sugawara T, Higashiyama N, Kaneyama S, et al. Multistep pedicle screw insertion procedure with patient-specific lamina fit-and-lock templates for the thoracic spine: clinical article. *J Neurosurg Spine*. 2013;19(2):185-190. doi:10.3171/2013.4.SPINE121059
18. Merc M, Drstvensek I, Vogrin M, Brajlilh T, Recnik G. A multi-level rapid prototyping drill guide template reduces the perforation risk of pedicle screw placement in the lumbar and sacral spine. *Arch Orthop Trauma Surg*. 2013;133(7):893-899. doi:10.1007/s00402-013-1755-0

19. Merc M, Drstvensek I, Vogrin M, Brajlilj T, Friedrich T, Recnik G. Error rate of multi-level rapid prototyping trajectories for pedicle screw placement in lumbar and sacral spine. *Chin J Traumatol*. 2014;17(5):261-266.
20. Merc M, Recnik G, Krajnc Z. Lumbar and sacral pedicle screw placement using a template does not improve the midterm pain and disability outcome in comparison with free-hand method. *Eur J Orthop Surg Traumatol*. 2017;27(5):583-589. doi:10.1007/s00590-017-1904-1
21. Putzier M, Strube P, Cecchinato R, Lamartina C, Hoff EK. A New Navigational Tool for Pedicle Screw Placement in Patients With Severe Scoliosis: A Pilot Study to Prove Feasibility, Accuracy, and Identify Operative Challenges. *Clin Spine Surg*. 2017;30(4):E430-E439. doi:10.1097/BSD.0000000000000220
22. Otsuki B, Takemoto M, Fujibayashi S, Kimura H, Masamoto K, Matsuda S. Utility of a custom screw insertion guide and a full-scale, color-coded 3D plaster model for guiding safe surgical exposure and screw insertion during spine revision surgery. *J Neurosurg Spine*. 2016;25(1):94-102. doi:10.3171/2015.12.SPINE15678
23. Hughes SP, Anderson FM. Infection in the operating room. *J Bone Joint Surg Br*. 1999;81(5):754-755. doi:10.1302/0301-620x.81b5.10370
24. Lu S, Zhang YZ, Wang Z, et al. Accuracy and efficacy of thoracic pedicle screws in scoliosis with patient-specific drill template. *Med Biol Eng Comput*. 2012;50(7):751-758. doi:10.1007/s11517-012-0900-1
25. Rosen C, Rothman S, Zigler J, Capen D. Lumbar facet fracture as a possible source of pain after lumbar laminectomy. *Spine*. 1991;16(6 Suppl):S234-238. doi:10.1097/00007632-199106001-00011
26. Puvanesarajah V, Jain A, Shimer AL, et al. Complications and Mortality Following 1 to 2 Level Lumbar Fusion Surgery in Patients Above 80 Years of Age: *SPINE*. 2017;42(6):437-441. doi:10.1097/BRS.0000000000001759
27. Malham GM, Wells-Quinn T. What should my hospital buy next?-Guidelines for the acquisition and application of imaging, navigation, and robotics for spine surgery. *J Spine Surg*. 2019;5(1):155-165. doi:10.21037/jss.2019.02.04
28. George E, Liacouras P, Rybicki FJ, Mitsouras D. Measuring and Establishing the Accuracy and Reproducibility of 3D Printed Medical Models. *RadioGraphics*. 2017;37(5):1424-1450. doi:10.1148/rg.2017160165
29. Popescu D, Laptoiu D. Rapid prototyping for patient-specific surgical orthopaedics guides: A systematic literature review. *Proc Inst Mech Eng H*. 2016;230(6):495-515. doi:10.1177/0954411916636919

30. Lau JC, Denning L, Lownie SP, Peters TM, Chen ECS. A Framework for Patient-Specific Spinal Intervention Simulation: Application to Lumbar Spinal Durotomy Repair. *Stud Health Technol Inform.* 2016;220:185-192.

## Chapter 4:

(a) Error measurement between Black-bone MRI-based and CT-based models;

(b) The Development of novel 2-in-1 patient specific, MRI-based 3D-printed laminectomy guides with integrated pedicle screw guides.

### Key words:

Lumbar spine.

3D-printing.

Image Processing, Computer-Assisted.

MRI.

Black-bone MRI

Pedicle screw.

Laminectomy.

### Introduction

CT is currently the gold-standard modality used to create spine bio-models and patient specific guides, although magnetic resonance imaging (MRI) is being used for this purpose in other orthopedic fields such as knee arthroplasty<sup>1-3</sup>. Currently, clinical spine MRIs are not precise enough to create 3D bio-models, due to excessive noise at the bone-soft tissue interface<sup>4</sup>.



Spine CT scans are often not required in the elective surgical setting, as MRI gives more pertinent information regarding the neural elements. Therefore, to create patient-specific guides, elective surgical candidates are often exposed to moderate amounts of radiation required for CT scans, purely for preoperative planning rather than diagnostic purposes. Theoretically, if the correct pre-operative diagnostic MRI data could be obtained, patient-specific guides could be created without the need for more data such as CT. The use of MRI, to create spinal bio-models and surgical guides, could avoid obtaining CT scans for planning purposes, and also avoid the need for additional radiation if intraoperative surgical navigation is used.

To our knowledge, there are no studies in the published literature which utilize MRI data to create spine bio-models and therefore no studies using MRI bio-models for creating patient-specific guides. Objectives of this study are to determine if accurate patient-specific spine surgical guides can be created from MRI data. An MRI sequence called the 'Black-bone' sequence, which is currently used to image pediatric skull deformities <sup>6</sup>, will be utilized as it has a relatively fast acquisition time, exhibits exquisite bone detail and minimizes noise at the bone-soft tissue interface ([Figure 1](#)). If bio-models can be created that are comparable to the 'ground-truth' (CT models), then our novel 2-in-1 laminectomy and pedicle screw guides will be created based on these models. These guides will be tested on cadaver spines to determine accuracy.

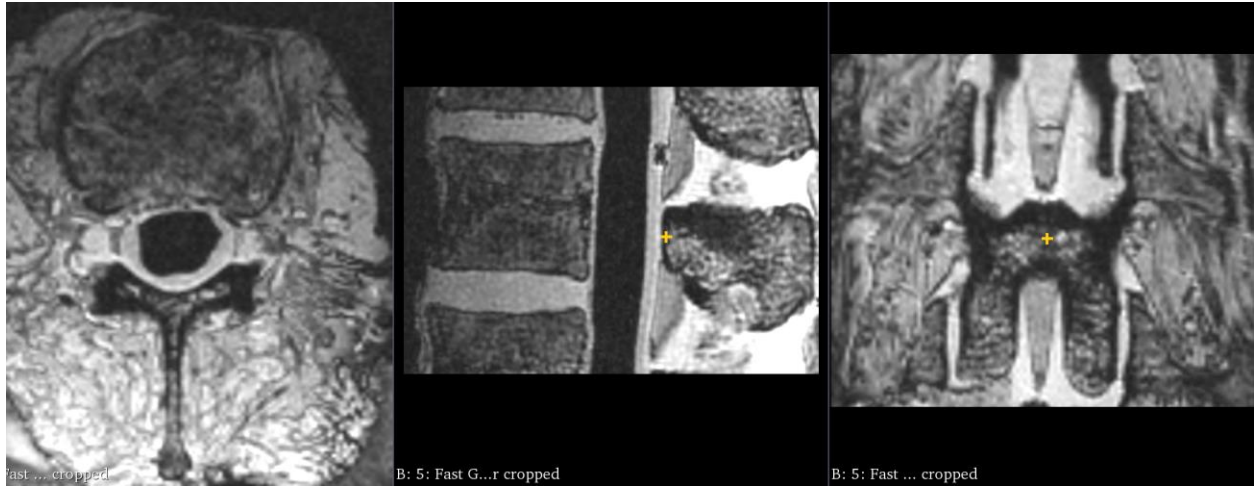


Figure 1

Axial, sagittal and coronal reconstructions of an L1 vertebra using the 'Black-bone' MRI sequence. Excellent bone details are demonstrated.

## Methods

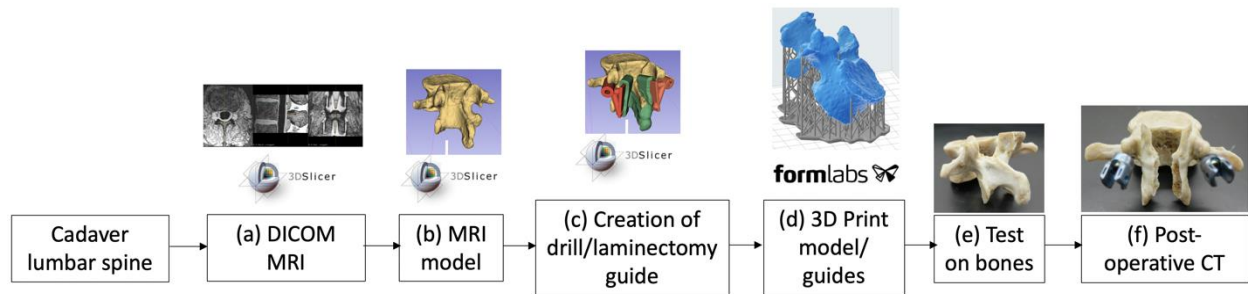


Figure 2

Overview of the image processing, 3D printing and testing steps. 3D Slicer software was obtained from slicer.org.

### Medical imaging (MRI and CT):

After institutional ethics approval, two complete human cadaver spines from Chapter 2 were harvested and imaged. MRI scans were obtained using GE Healthcare 3T Discovery MR750 scanner. The soft tissues, including the paraspinal muscles circumferentially, were left intact during the scanning processes, in order to replicate the clinical scenario as much as possible.

A 'Black-bone' sequence ([Figure 1](#), [Figure 2a](#)) was acquired with parameters outlined in [Table 1](#). The scans were examined to exclude pathology causing any anatomical distortion. Scan times for this sequence are approximately 6 minutes.

Imaging Plane:	Sagittal
Imaging Mode:	3D
Pulse Sequence:	Gradient Echo
Imaging Options:	Fast
Frequency Field of View:	240 mm
Phase Field of View:	60 % or 144 mm
Frequency Matrix:	384 mm
Phase Matrix:	384 mm
Slice Thickness:	0.6 mm
Slice Overlap:	None; NEX: 3
Flip Angle:	5 Degrees
TR:	7.4 ms
TE:	3.1 ms
Receive Bandwidth:	+/- 62.50 kHz
Frequency Direction:	S/I

Table 1

The MRI parameter for the 'Black-bone' sequence.

For MRI to CT model comparison, CT scans were obtained using the same protocol as in

[Chapters 2](#) and [3](#).

#### Soft tissue removal:

The cleaned bones from 2 of the spine described in [Chapter 2](#) were utilised.

#### Images processing, segmentation and creation of patient-specific guides:

3D mesh models were created by importing the MRI digital imaging and communication in medicine (DICOM) files into 3D Slicer version 4.10.2 ([www.slicer.org](http://www.slicer.org), Figure 2b).

Each vertebral model was created using the same methods as in [Chapter 3](#), except the semi-automated 'watershed' extension in the Segment Editor of 3D Slicer ([Figure 3a](#)) was used instead of the 'grow-from-seeds' extension. The segmentation of the MRI scan was performed prior to the segmentation of the CT scan or cleaning of the bones, in order to reduce bias from prior knowledge of the 'ground-truth' model. The vertebral bodies and transverse processes were excluded from the segmentation as the lack of soft tissues in these areas made the cortical bone margins less distinct. The final model was exported as a STL file. The MRI models were designated (MRM).

The CT scan DICOM was used to create models with the same methods as [Chapters 2](#) and [3](#) and designated as CTM.

PSGs were constructed using the same methods as used in [Chapter 3](#) ([Figure 2c](#), [Figure 3](#)).

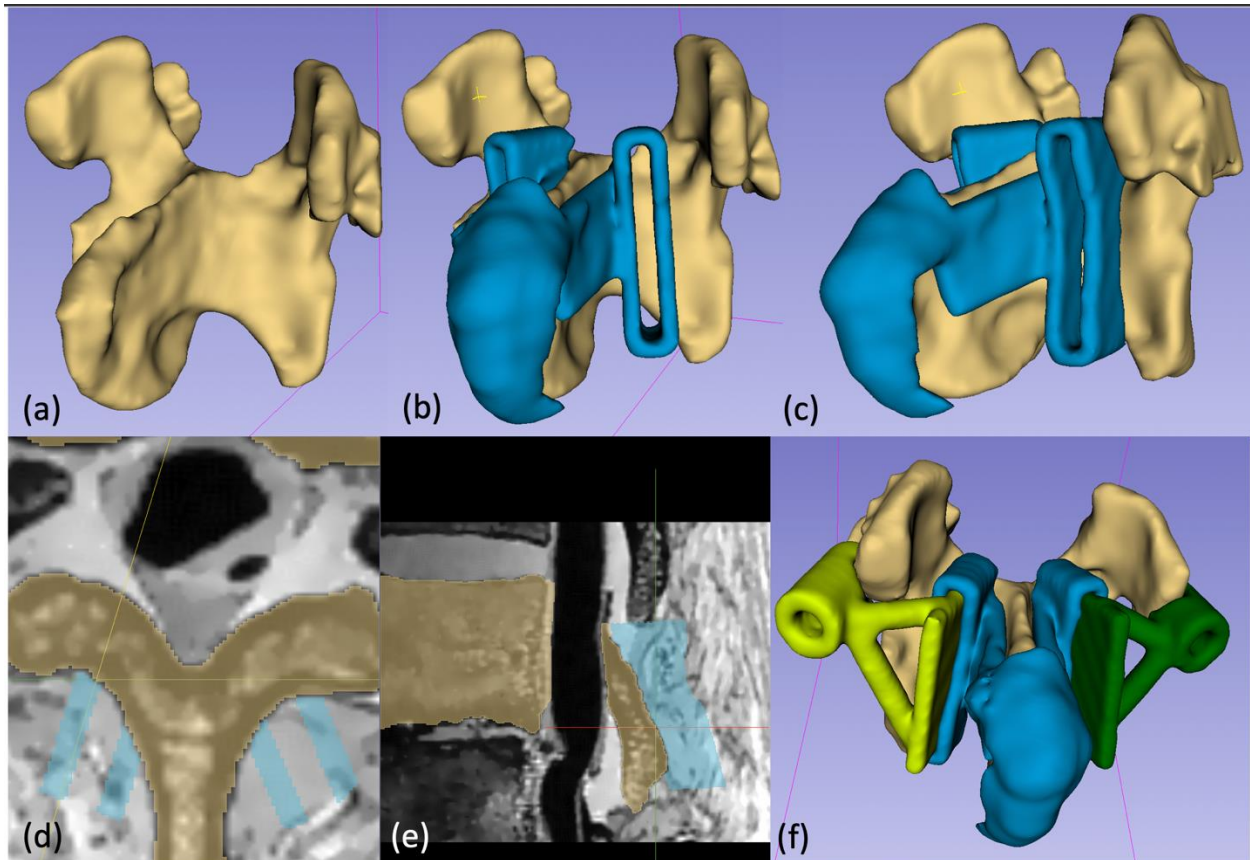


Figure 3

(a) A 3D model of the vertebra was created from 'Black-bone' MRI data, using 3D Slicer. (b), (c) Longitudinal laminectomy guides were placed in the appropriate position and connected to a template placed on the spinous process. (d) and (e) Axial and sagittal reconstructions demonstrating how the laminectomy guides were designed to match the deep surface of lamina, to create a depth-stop design. (f) Removable drill guides were created to assist in pedicle screw insertion and joined to slots which fit into the laminectomy guides, to create a 2-in-1 guide.

3D-printing of PSGs (Figure 2d):

3D-printing settings were the same methods as used in [Chapters 2](#) and [3](#).

#### Measurements:

The 2 model types were compared: (1) CTM; and (2) MRM. Limited measurements were made using similar methodology to that in Chapter 2. Several measurements could not be assessed due to the exclusion of the vertebral bodies and transverse processes from the segmentation. The included measurements were as follows: Left and right vertebral height, spinous process length and height, and right and left pedicle height and width.

When acquiring segmentation metrics, the CT and MRI models were aligned using the same methods in [Chapters 2](#) and [3](#). The aligned models were cropped by focusing a region-of-interest around the bases of the transverse process and vertebral bodies. This ensured that there was a standardized anatomical coverage across the MRI and CT models.

#### Pre-operative assessment:

The parameters set out in Chapter 3 were recorded ([Table 1](#)).

#### Testing of the PSGs:

Testing of the PSGs was performed using the same techniques described in [Chapter 3](#).

Intraoperative assessment:

Intraoperative assessment was performed using the same techniques described in [Chapter 3](#).

Postoperative assessment ([Table 2](#)):

Postoperative assessment was performed using the same techniques described in [Chapter 3](#).

Statistical analysis:

Means and standard deviation for continuous variables are presented. Statistical analysis was performed with SPSS software ver. 20.0 (SPSS Inc., Chicago, IL), using one-way ANOVA (AB, 3DSM, CTM, 3DP, MRM), and a paired student's T-test was used to compare the CTM and MRM models.

A paired student's T-test was used to compare the planned and actual laminectomy distances, as well as the remaining width of the mid-pars interarticularis.  $P \leq 0.05$  were considered statistically significant.



## Results

### Segmentation measurements and metrics:

11 vertebrae were included in this analysis, as one specimen had a lumbarized S1.

There were no statistical differences between manual measurements when comparing the MRM to the other 4 model types ( $p = 0.247$ ), except for the height of the spinous process and the left pedicle height ([Figure 4](#)). There was no significant difference between MRM and CTM, when comparing the average of all measurements ( $p = 0.435$ ).

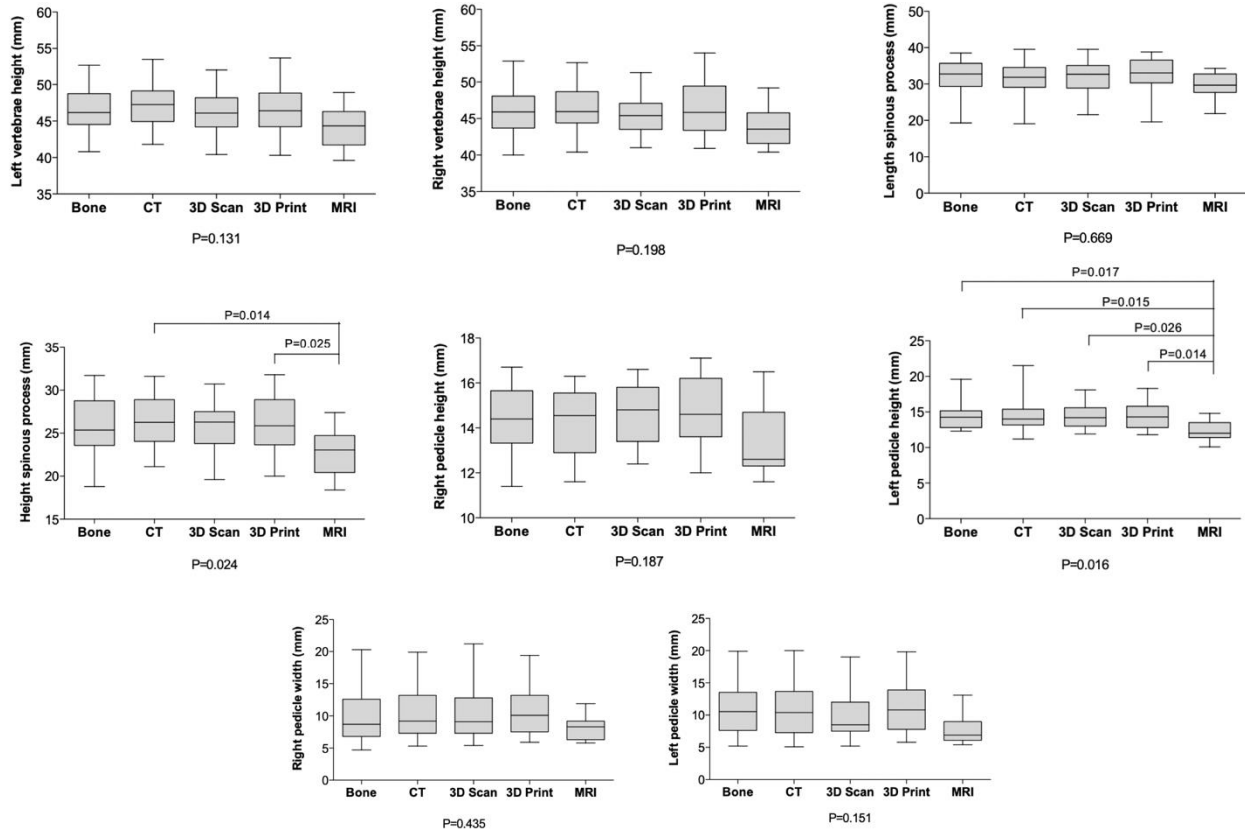


Figure 4

Box and whisker plots for manual vertebral measurements. There were no statistical differences between manual measurements when comparing the MRM to the other 4 model types, except for the height of the spinous process ( $p = 0.025$ ) and the left pedicle height ( $p = 0.017$ ).

The mean Dice Coefficient was 0.89 (SD 0.009) when comparing MRM to CTM, indicating excellent geometric overlap. The mean Hausdorff distance was 0.38 mm (SD 0.03mm) when comparing MRM to CTM, signifying approximately 0.4mm difference between the 2 models ([Figure 5c-e](#)). The mean volume for MRM and CTM were 10.9ml and 11.2ml ( $p = 0.09$ ), respectively, indicating no significant difference between the mean volumes of the 2 models.

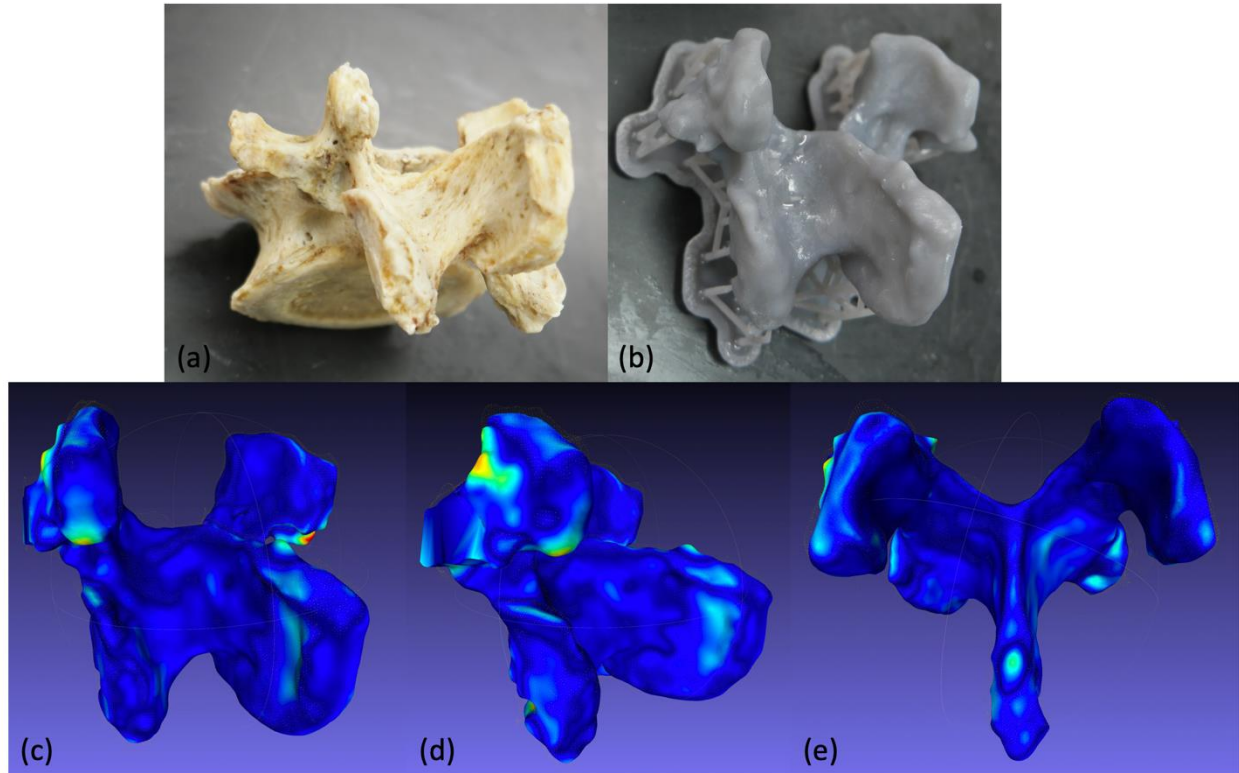


Figure 5

(a) Left posterolateral aspect of an L3 vertebra (same bone as in Figure 3). (b) 3D printed model of the posterior vertebral elements using MRI data. (c - e) Digital comparison between the CT and MRI models. The green and yellow areas indicate subtle difference between the 2 model types.

Variable	Result	
Cortical breaches	0	
Mean axial screw error	1.0 deg	SD 1.6
Mean sagittal screw error	0.6 deg	SD 1.2
Mean distance deviation at pedicle midpoint	0.79 mm	SD 0.4
Deep Laminectomy passes	2	
Average surgical time	4min 48 sec	54 sec
Average vertebral segmentation time	58 min	SD 6.7 min
Average template design time	57 min	SD 10 min
Average vertebral print time	3 h 36 min	SD 16 min
Average template print time	3 h 20 min	SD 18 min
Average vertebral print volume	15.0 ml	SD 3.3 ml
Average template print volume	14.0 ml	SD 1.4 ml
	Planned	Actual
Cranial laminectomy width	10.1 mm	11.3 mm (p < 0.05)
Caudal laminectomy width	12.2 mm	13.3 mm (p < 0.05)
Width of pars-interarticularis	7.4 mm	6.8 mm (p < 0.05)

Table 2  
Summary of results.

### Screw analysis (Table 2):

In total, 22 screws were inserted in 11 lumbar vertebrae, by using the integrated 2-in-1 patient-specific drill guides. There were no cortical breaches on direct examination, or on postoperative CT (grade 0), in any case or in any direction. The mean axial screw error was 1.0 degrees (SD 1.6). The mean sagittal screw error was 0.6 degrees (SD 1.2). The mean distance deviation between planned and actual screw position at the midpoint of the pedicle in the coronal plane was 0.79mm (SD 0.4).

### Laminectomy analysis (Table 2):

Digital video analysis revealed the burr tip passed deep to the inner table margin in 2 of the 22 laminae. On postoperative inspection of the laminectomy guides, both guides had split in their cranial portion, most likely due to vibration from the burr. This led to separation of the medial and lateral portions of the laminectomy guide which allowed the burr to travel deep to the inner margin of the lamina by approximately 2mm.

There was a significant difference between mean planned and actual width of cranial aspect of the laminectomy, measuring 10.1mm and 11.3mm, respectively ( $p < 0.01$ ). There was a significant difference between the mean planned and actual width of caudal aspect of the laminectomy, measuring 12.2mm and 13.3mm, respectively ( $p < 0.01$ ). There was a significant

difference between mean planned and actual remaining width of the mid-pars interarticularis, measuring 7.4mm and 6.8mm, respectively ( $p < 0.01$ ).

#### Surgical times and print parameters (Table 2):

Average surgical time was 4 minutes and 48 seconds (SD 54s), per level, including positioning of guides, bilateral screw insertion and laminectomy, for 11 vertebrae.

The average segmentation time for the vertebral model and corresponding template set was 58 mins (SD 6.7), and 57 mins (SD 10) respectively, for 11 vertebrae.

The average print time for the vertebral model and corresponding template set was 3 hours 36 mins (SD 16 mins) and 3 hours 20 mins (SD 18), respectively, for 11 vertebrae.

The average print volume for the vertebral model and corresponding template set was 15.0 ml (SD 3.3) and 14.0ml (SD 1.4), for 11 vertebrae.

#### Discussion

With the increasing use of 3D-printing in medicine, there is a need for high-quality 3D images for surgical planning. The cumulative lifetime radiation dose of the population needs to be minimized by reducing the exposure to ionizing radiation<sup>5</sup>. CT is the current gold standard

modality in orthopedic 3D-printing because of its speed of image acquisition and ease of bone segmentation, however radiation-free imaging modalities are increasingly being sought <sup>6</sup>. Using MRI for 3D-printing is more difficult because of the heterogenous signal intensities in tissues and poor signal to noise ratios <sup>7</sup>.

#### General orthopedic segmentation using MRI data:

MRI data use for 3D-printing is commonly used the field of general orthopedics. Several meta-analyses comparing imaging modalities in total knee arthroplasty demonstrate that MRI-based guides were at least as good, if not better than CT-based guides at reducing alignment outliers <sup>8</sup> <sup>9</sup>. Additionally, patient-specific instrumentation has been shown to be at least as good, if not better than conventional instrumentation. Pre-operative planning allows determination of resection margins, and implant size and position, in order to improve component alignment and ultimately revision rates <sup>3</sup> <sup>10</sup>.

#### Spine segmentation using MRI data:

There has been a rise in publications on computerized methods for spine analysis on MRI <sup>7,11-13</sup>, with work focused of segmentation of vertebral bodies, intervertebral discs, spinal canal and spinal cord. However, the segmentation of any anatomic structure using MRI is a demanding process which requires large amounts of manual editing. There are sparse publications examining fully automated segmentation algorithms of the spine <sup>7,14</sup>. Errors of 2.0 +/- 0.8mm

were reported for fully automated MRI-based spine models compared to CT, which could be problematic if these segmentation techniques are applied to use of PSGs. Semi-automatic segmentation techniques, such as thresholding, seed growing and edge detection, are extremely effective when using CT data, however no single technique is currently useful when segmenting MRI data. As image contrast and quality do not allow for a single technique, several semi-automated techniques, in combination with manual segmentation, are necessary to create models using MRI data. Several publications have examined segmentation of vertebral bodies using clinical MRI <sup>12,13</sup>, with good results compared to the ground-truth (manual segmentations segmented slice-by-slice by expert radiologists or surgeons). However, these studies used clinical T2 sequences, which do not offer enough detail to use for PSGs.

There has been a lack of focus on MRI-based segmentation of the neural arch structures with a view to create bio models which can be used for patient-specific instrumentation. In practice, clinical MRI scan sequences target the spinal canal and neural structures, due to their different properties when compared to the vertebrae and discs. Therefore, if clinical MRI scans were to be utilized for segmentation of vertebrae then the additional sequences would need to be added (such as fast-GRE/‘black-bone’ or ultrashort echo time sequences).

The qualitative appearance of the bio-models in our study was excellent ([Figures 3](#) and [5](#)). We found the best results were obtained from the ‘watershed’ technique in the Segment Editor extension of 3D Slicer. The ‘watershed’ technique is a semi-automated segmentation technique which is obtained in a similar manner to the ‘grow-from-seeds’ technique, however, it gives



smoother and more well-defined segments which is ideal when using MRI data. The disadvantage of using this technique is that it is more time consuming than the 'grow-from-seeds' technique, especially when seeds need to be modified. As well as the qualitative appearance, we found excellent geometric similarities between the MRI models and CT models, which is contrary to previous publications <sup>1</sup>.

The 'black-bone' MRI sequence has been used previously in the craniofacial skeleton, to offer a non-ionizing alternative to CT in children with skull abnormalities <sup>6 15</sup>. Robinson et al. found that fetal 'black-bone' MRI could be used in the assessment of spinal abnormalities, therefore reducing the risks of ionizing radiation to the mother and the fetus <sup>16</sup>. Eley et al. were the first to accurately 3D-print a range of human skulls from 'black-bone' MRI data. This sequence minimizes soft tissue contrast, to improve definition at the bone-soft tissue interface, rather than traditional sequences used to highlight bony anatomy which increase signal intensity from the bone (e.g. Ultrashort echo time (TE)). To our knowledge, ours is the first study to utilize MRI data to create and successfully test spine patient-specific guides.

The 'black-bone' technique utilizes a gradient echo (GRE) sequence, such as the 3D fast GRE (GE systems), with a short TE (4.2ms)/ repetition time (8.6ms) and a flip angle of 5 degrees with a 1.5T or 3.0T magnet. The main limitation of the technique is imaging bone that comes into contact with air, since both return little to no signal. Therefore, in this cadaveric study, segmentation of the transverse processes and vertebral bodies was problematic, and therefore excluded, as the spines were already harvested from the donors. Fortunately, these surfaces

are not used for surface matching of PSGs in the lumbar spine. Therefore, the potential remains to use these sequences in clinical practice to create spine bio models and PSGs. This may eventually obviate the need for pre-operative spinal CT scans for PSG production.

We found excellent spatial agreement and geometric overlap when comparing MRM to CTM, with high Dice Coefficients and no statistical difference between volumetric comparisons. This is contrary to several studies looking at comparisons of the knee joint, where on average the CT models are slightly larger than the MRI models. Neubert et al. found this difference due to the lack of hydrogen in cortical bone thereby reducing its profile <sup>2</sup>. The difference between these studies and ours is likely due to the improved image quality at the cortical bone margin when using the 'Black-bone' sequence. Nevertheless, the 'Black-bone' sequence will need to be performed in the clinical setting, in order to determine if it can accurately image in vivo spinal anatomy. This will be necessary before any further clinical testing can be performed.

#### Time utilisation:

MRI acquisition is currently time consuming, and in the clinical setting, motion artefact is more likely to result <sup>1</sup>. Even a relatively quick GRE acquisition time of 4-5 minutes, still cannot compete with the matter of seconds it takes to acquire a CT data set <sup>6</sup>.

The segmentation of spinal models from MRI scans is also more time consuming than using CT scans, because of the manual editing required. This in itself creates more room for error as the

process becomes more user dependent. The average time taken to segment a vertebra from our CT data takes 33 mins ([Chapter 3](#)), compared to 58 mins for MRI segmentations. Fully automated processes using deep learning could achieve segmentation times that are comparable to CT<sup>7,14</sup>. The process of creating templates was slightly faster in the MRI group (57 mins versus 77 mins), which is likely due to the learning curve in using 3D Slicer.

#### Cost of production:

Surgical guide resin retails for US \$149 per litre. Therefore, the material cost of one vertebral model is approximately US \$2.24, and one template set costs approximately US \$2.10.

#### Limitations:

This cadaveric study does not represent surgery in many ways. The use of cadaver spines eliminated the issues of motion and flow artefacts which can be seen in the clinical setting. The bones were meticulously cleaned, which is time consuming and only possible intra-operatively to a lesser degree. The cleaning, however, provided an accurate representation of the spinal canal during laminectomy which has not been studied before. The novel use of digital video recording to assess laminectomy safety has not been validated and does not guarantee that the burr tip will not cause damage to the dura or neural elements clinically. However, we believe it is currently the best possible way to assess this new technique. The use of a side cutting burr with a blunt tip, such as the match head burr, minimises dura or neural injury even if contact

occurs. Nevertheless, it is extremely difficult to recreate a realistic dural tube in the cadaveric laboratory setting <sup>17</sup>, and may require animal tests to determine safety before use on humans.

Despite a significant difference found when comparing the planned and actual laminectomy widths and amount of pars remaining, the mean differences were all approximately 1mm which is not clinically significant. The mean of 1.4mm over-resection of bone from the pars, is likely due to the medial-lateral angular tolerance allowed in the laminectomy guide, which is not clinically significant. A mean of 6.8mm of mid-pars interarticularis remained, which reduces the risk of iatrogenic pars fracture and spondylolisthesis <sup>18</sup>.

3D Slicer is an open-source software which can be used for research studies. It has several powerful segmentation tools and is capable of creating models and guides via the 'Segment Editor' and 'Create Models' extensions. It is currently not FDA approved to be used in the clinical setting, therefore, to reproduce this study clinically, a similar FDA approved segmentation tool, such as MIMICS (Materialize, Leuven Belgium), would need to be utilized.

## Conclusion

This study confirms that it is possible to create accurate spine bio-models using semi-automatic segmentation of MRI data. The patient-specific 2-in-1 laminectomy and pedicle drill guides created from this data were used to successfully carry out complex surgical steps in a timely

fashion. More research will be necessary to determine if the 'Black-bone' MRI sequence can be useful in the clinical setting to aide in production of PSGs.

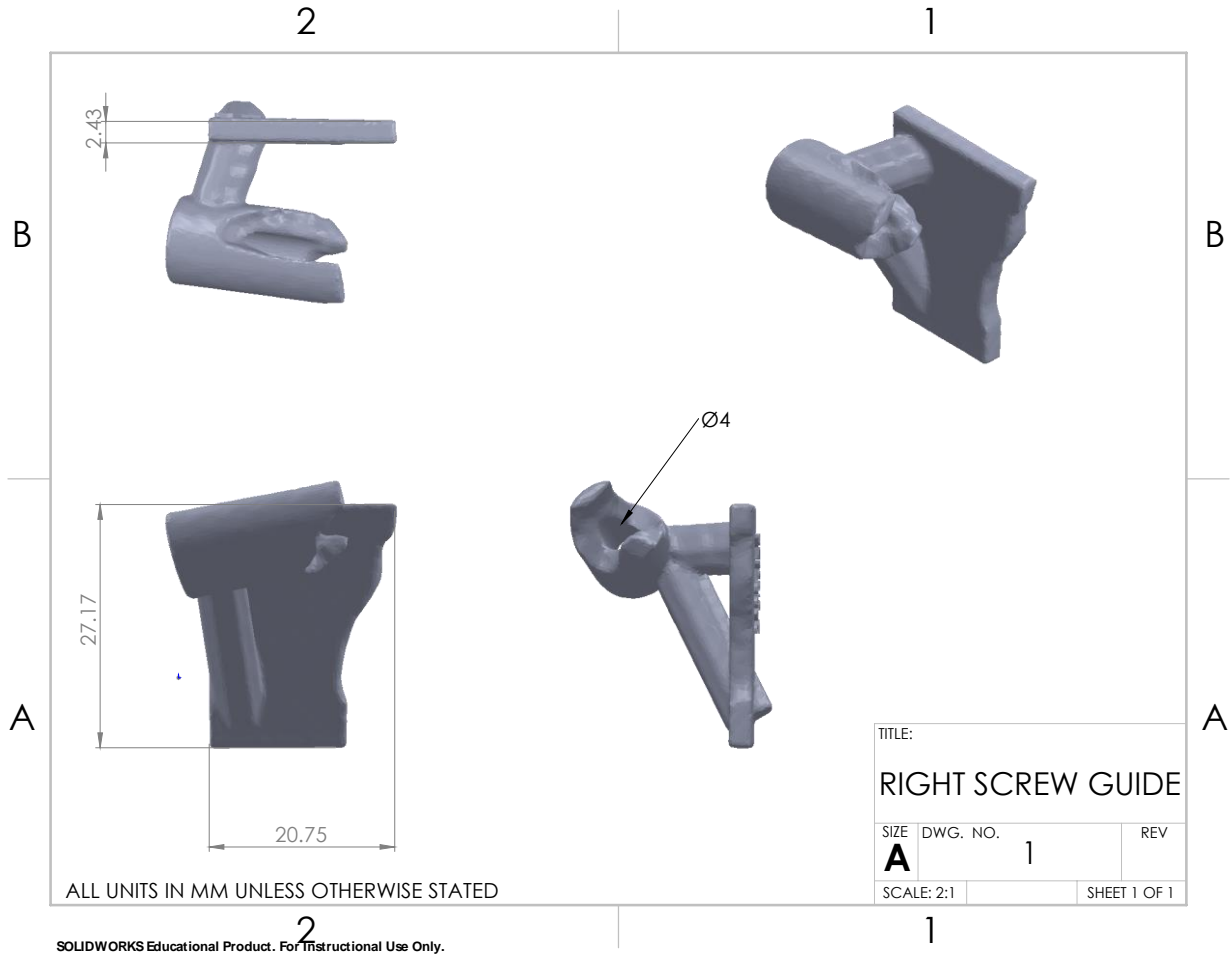
#### Chapter 4 reference list

1. White D, Chelule KL, Seedhom BB. Accuracy of MRI vs CT imaging with particular reference to patient specific templates for total knee replacement surgery. *Int J Med Robotics Comput Assist Surg.* 2008;4(3):224-231. doi:10.1002/rcs.201
2. Neubert A, Wilson KJ, Engstrom C, et al. Comparison of 3D bone models of the knee joint derived from CT and 3T MR imaging. *European Journal of Radiology.* 2017;93:178-184. doi:10.1016/j.ejrad.2017.05.042
3. Stirling P, Valsalan Mannambeth R, Soler A, Batta V, Malhotra RK, Kalairajah Y. Computerised tomography vs magnetic resonance imaging for modeling of patient-specific instrumentation in total knee arthroplasty. *World J Orthop.* 2015;6(2):290-297. doi:10.5312/wjo.v6.i2.290
4. Popescu D, Laptoiu D. Rapid prototyping for patient-specific surgical orthopaedics guides: A systematic literature review. *Proc Inst Mech Eng H.* 2016;230(6):495-515. doi:10.1177/0954411916636919
5. van Eijnatten M, Rijkhorst E-J, Hofman M, Forouzanfar T, Wolff J. The accuracy of ultrashort echo time MRI sequences for medical additive manufacturing. *Dentomaxillofac Radiol.* 2016;45(5):20150424. doi:10.1259/dmfr.20150424
6. Eley KA, Watt-Smith SR, Golding SJ. "Black Bone" MRI: a novel imaging technique for 3D printing. *Dentomaxillofacial Radiology.* 2017;46(3):20160407. doi:10.1259/dmfr.20160407

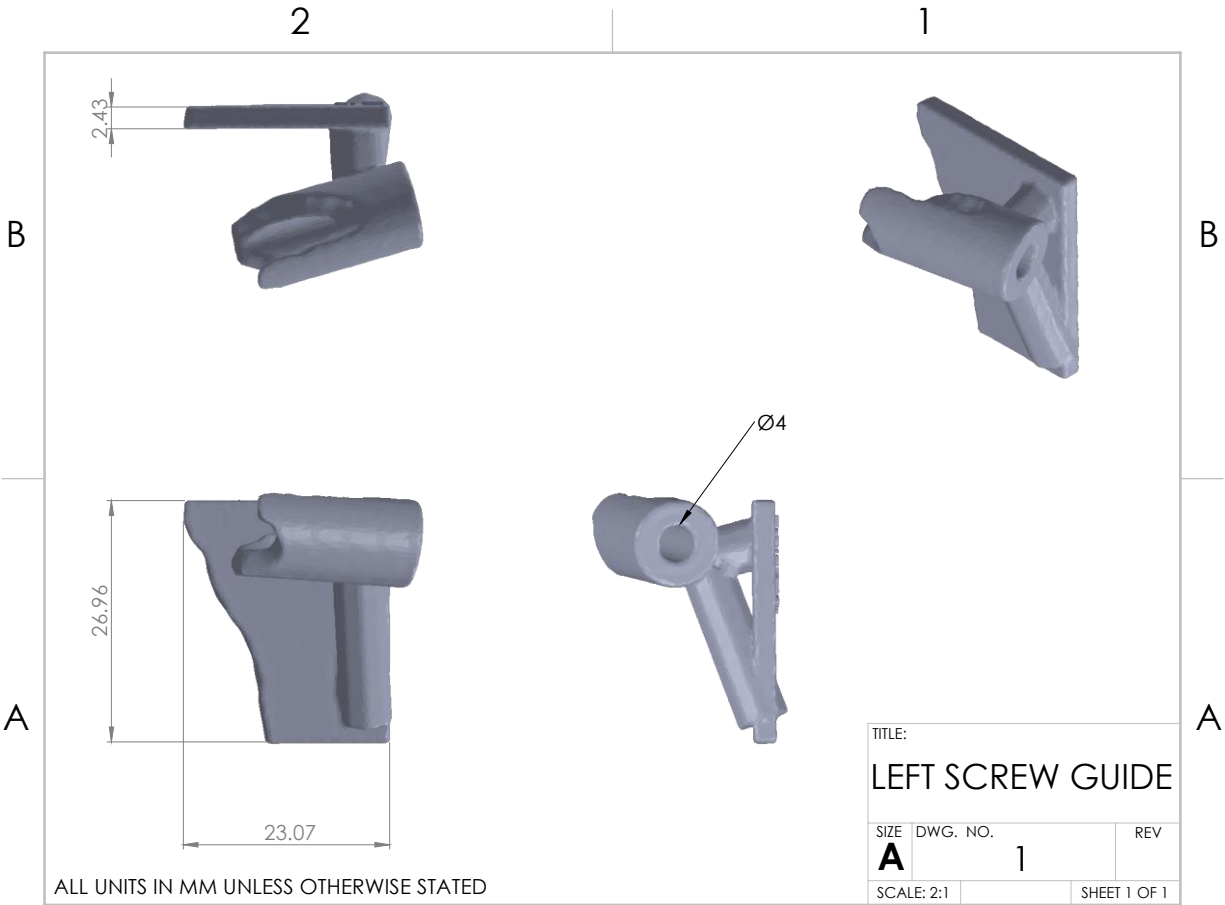
7. Hoad CL, Martel AL. Segmentation of MR images for computer-assisted surgery of the lumbar spine. *Phys Med Biol*. 2002;47(19):3503-3517. doi:10.1088/0031-9155/47/19/305
8. Schotanus MGM, Thijs E, Heijmans M, Vos R, Kort NP. Favourable alignment outcomes with MRI-based patient-specific instruments in total knee arthroplasty. *Knee Surg Sports Traumatol Arthrosc*. 2018;26(9):2659-2668. doi:10.1007/s00167-017-4637-0
9. An VVG, Sivakumar BS, Phan K, Levy YD, Bruce WJM. Accuracy of MRI-based vs. CT-based patient-specific instrumentation in total knee arthroplasty: A meta-analysis. *J Orthop Sci*. 2017;22(1):116-120. doi:10.1016/j.jos.2016.10.007
10. Asada S, Mori S, Matsushita T, Nakagawa K, Tsukamoto I, Akagi M. Comparison of MRI- and CT-based patient-specific guides for total knee arthroplasty. *The Knee*. 2014;21(6):1238-1243. doi:10.1016/j.knee.2014.08.015
11. Rak M, Tönnies KD. On computerized methods for spine analysis in MRI: a systematic review. *Int J CARS*. 2016;11(8):1445-1465. doi:10.1007/s11548-016-1350-2
12. Egger J, Nimsky C, Chen X. Vertebral body segmentation with *GrowCut* : Initial experience, workflow and practical application. *SAGE Open Medicine*. 2017;5:205031211774098. doi:10.1177/2050312117740984
13. Hille G, Saalfeld S, Serowy S, Tönnies K. Vertebral body segmentation in wide range clinical routine spine MRI data. *Computer Methods and Programs in Biomedicine*. 2018;155:93-99. doi:10.1016/j.cmpb.2017.12.013
14. Kadoury S, Labelle H, Paragios N. Spine segmentation in medical images using manifold embeddings and higher-order MRFs. *IEEE Trans Med Imaging*. 2013;32(7):1227-1238. doi:10.1109/TMI.2013.2244903

15. Eley KA, Watt-Smith SR, Golding SJ. "Black Bone" MRI: a potential non-ionizing method for three-dimensional cephalometric analysis--a preliminary feasibility study. *Dentomaxillofac Radiol.* 2013;42(10):20130236. doi:10.1259/dmfr.20130236
16. Robinson AJ, Blaser S, Vladimirov A, Drossman D, Chitayat D, Ryan G. Foetal "black bone" MRI: utility in assessment of the foetal spine. *Br J Radiol.* 2015;88(1046):20140496. doi:10.1259/bjr.20140496
17. Lau JC, Denning L, Lownie SP, Peters TM, Chen ECS. A Framework for Patient-Specific Spinal Intervention Simulation: Application to Lumbar Spinal Durotomy Repair. *Stud Health Technol Inform.* 2016;220:185-192.
18. Rosen C, Rothman S, Zigler J, Capen D. Lumbar facet fracture as a possible source of pain after lumbar laminectomy. *Spine.* 1991;16(6 Suppl):S234-238. doi:10.1097/00007632-199106001-00011

Appendix  
Engineering drawings



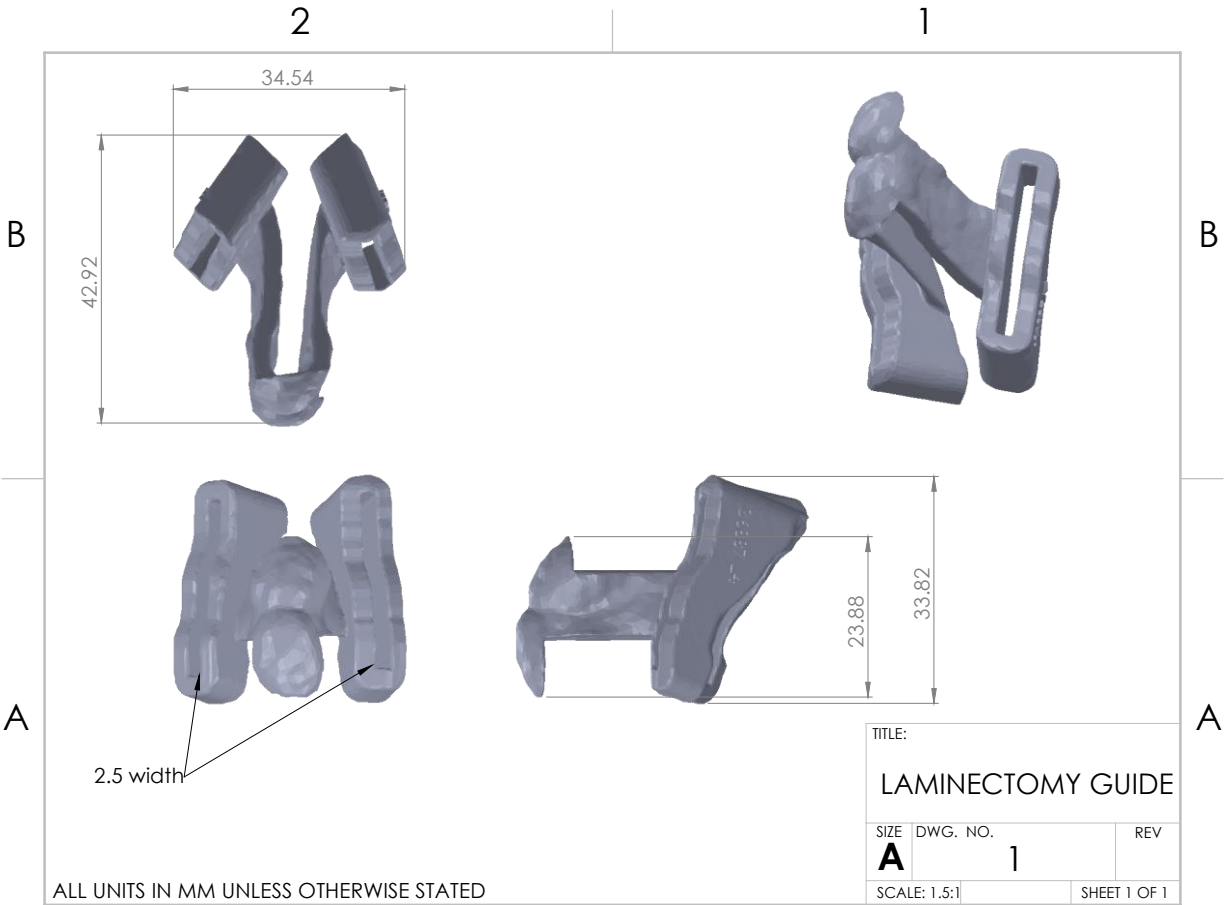




ALL UNITS IN MM UNLESS OTHERWISE STATED

2  
SOLIDWORKS Educational Product. For Instructional Use Only.

1



SOLIDWORKS Educational Product. For Instructional Use Only.

## Curriculum Vitae

ANDREW KANAWATI

Orthopaedic Surgeon (FRACS Orth)

2018

### Employment:

2018 – Current: Spine Fellow, Victoria Hospital, London, Ontario, Canada

2018 – Consultant Orthopaedic Surgeon Westmead Hospital Sydney

2009 – 2017: AOA Orthopaedic Trainee

2008 – 2009: Resident Medical Officer - South West Sydney Area Health Service

2007 – 2008: Intern - South West Sydney Area Health Service

### Presentations:

2018 – AOA National ASM – Non-operative management of greater trochanter fractures.

Presented by Annabel Probert.

2017 - Australia Orthopaedic Trauma Society ASM – Distance of the femoral neurovascular bundle from the hip joint. Presented by Cyrus Mehta.

2016 –Australian Orthopaedic Registrars Association – Allan Frederick Dwyer Prize for Best Scientific Paper Runner-up

Safe zone for the superficial femoral artery demonstrated on computed tomography angiography.

AOA National ASM Meeting 2016 – ‘The effect of Gluteus Maximus tendon release on the position of the sciatic nerve during the posterior approach to the hip’

AOA NSW Branch Meeting 2016 – ‘The Distance of the Common Peroneal Nerve to the Posterolateral Structures of the Knee’.

2015 – Winner 2015 Australian Orthopaedic Registrars Association – Allan Frederick Dwyer Prize for Best Scientific Paper

The change in position of the sciatic nerve during the posterior approach to the hip.

AOA National ASM and NSW AOA Branch Meeting 2015 – ‘The change in position of the sciatic nerve during the posterior approach to the hip’

RACS SRS Meeting 2015 – ‘The change in position of the sciatic nerve during the posterior approach to the hip’

2009 – National ASM and NSW AOA Branch Meeting - ‘The Non-operative Treatment of Patella Fractures without Splinting’

Post-graduate study:

2017 – FRACS Orth

2015 – Master of Anatomy by Dissection, University of New England

2013 – Graduate Diploma of Anatomy by Dissection, University of New England

2011 – Graduate Certificate of Anatomy by Dissection, University of New England

Publications:

The change in position of the axillary nerve with rotation of the arm.

Olivia Fox Peter Lorentzos Moussa Farhat Andrew Kanawati

Clin Anat 2018 Oct 10. Epub 2018 Oct 10.

Extensile lateral versus sinus tarsi approach for displaced, intra-articular calcaneal fractures: a meta-analysis.

Mehta CR, An VVG, Phan K, Sivakumar B, Kanawati AJ, Suthersan M.

J Orthop Surg Res. 2018 Sep 24;13(1):243. doi: 10.1186/s13018-018-0943-6. Review.

PMID: 30249288

The distance of the femoral neurovascular bundle from the hip joint: an intraoperative guide to reduce iatrogenic injury.

Mehta CR, Constantinidis A, Farhat M, Suthersan M, Graham E, Kanawati A.

J Orthop Surg Res. 2018 Jun 4;13(1):135. doi: 10.1186/s13018-018-0847-5

PMID: 29866137

The Distance of the Common Peroneal Nerve to the Posterolateral Structures of the Knee.

Jenkins MJ, Farhat M, Hwang P, Kanawati AJ, Graham E.

J Arthroplasty. 2016 May 12. pii: S0883-5403(16)30139-5. doi: 10.1016/j.arth.2016.05.005.

[Epub ahead of print]

PMID: 27267229

Safe zone for the superficial femoral artery demonstrated on computed tomography angiography.

Narulla RS, Kanawati AJ.

Injury. 2016 Mar;47(3):748-51. doi: 10.1016/j.injury.2015.12.012. Epub 2015 Dec 29.

PMID: 26775209

Lunate-triquetral coalition in an Australian setting.

Hinde YR, Amali D, Kanawati A.

ANZ J Surg. 2015 Dec 17. doi: 10.1111/ans.13382. [Epub ahead of print]

PMID: 26678244

The change in position of the sciatic nerve during the posterior approach to the hip.

Kanawati AJ, Narulla RS, Lorentzos P, Facchetti G, Smith A, Stewart F.

Bone Joint J. 2015 Aug;97-B(8):1056-62. doi: 10.1302/0301-620X.97B8.35746.

PMID: 26224821

iatrogenic patellar tendon deficiency treated with rectus femoris tendon turndown autograft.

Kanawati AJ, Stening M.

ANZ J Surg. 2015 Mar 12. doi: 10.1111/ans.13012. [Epub ahead of print]

PMID: 25765869

The influence of entry point and radius of curvature on femoral intramedullary nail position in the distal femur.

Kanawati AJ, Jang B, McGee R, Sungaran J.

J Orthop. 2014 May 14;11(2):68-71. doi: 10.1016/j.jor.2014.04.010. eCollection 2014 Jun.

PMID: 25104888

Variations of the sciatic nerve anatomy and blood supply in the gluteal region: a review of the literature.

Kanawati AJ.

ANZ J Surg. 2014 May 20. doi: 10.1111/ans.12675. [Epub ahead of print]

PMID: 24842563

Laser etching causing fatigue fracture at the neck-shoulder junction of an uncemented femoral stem: A case report.

Jang B, Kanawati A, Brazil D, Bruce W.

J Orthop. 2013 May 24;10(2):95-8. doi: 10.1016/j.jor.2013.04.007. eCollection 2013.

PMID: 24403758

Courses:

- 2015 – Argo Exeter Course – Brisbane, Australia
- 2014 - Registrar Hand Surgery Review Course – Gold Coast, Australia
- 2014 - ARGO Hip Arthroplasty Cadaver Course, Brisbane, Australia
- 2013 - APOS Instructional Course, Sunshine Coast, Australia
- 2013 – AO Advanced Principles of Fracture Management – Sydney, Australia
- 2011 – Upper and Lower Limb Trauma Dissection Course, University of Melbourne
- 2010 - AO Trauma Course - Paediatric
- 2010 - AO Spine Principles Course on Spinal Trauma & Lumbar Degeneration
- 2010 - CLEAR Course - Oriental Bay, NZ
- 2009 - Sydney Clinical Skills and Simulation Centre Arthroscopic Surgery Skills Workshop
- 2009 - AO Principles in Operative Fractures Management - Sydney, Australia
- 2009 - CCrISP Course - St George Hospital, NSW
- 2009 - EMST Course - Liverpool Hospital, NSW
- 2009 - ASSET Course - RACS Education Centre, Melbourne

Teaching:

- 2013 – 2015 Senior Lecturer UNE Department of Rural Medicine
- 2010 -2011- Clinical Examiner UWS, Blacktown/Mt Druitt Clinical School



2009 - Bedside Tutor/Clinical Examiner UNSW, South Western Sydney Clinical School, Liverpool  
Hospital

2003-2004 Medical Anatomy Tutor UNSW - Musculoskeletal Anatomy, Head and Neck  
Anatomy, Neuroanatomy, Visceral Anatomy

Education:

Tertiary Education: 2006 - MBBS (Honours Class 2 Division 2)

Secondary Education: 2000 - HSC, UAI 99.70

Extra-curricular:

2008-2009 Liverpool Hospital RMO Association President

2006-2007 Army Reserves Medical Assistant, Rank - Private